Exploring macroevolutionary links in multi-species planktonic foraminiferal Mg/Ca and δ^{18}O from 15 Ma to Recent

Flavia Boscolo-Galazzo[1*], David Evans[2], Elaine M. Mawbey[3], William R. Gray[4], Paul N. Pearson[3,5], Bridget S. Wade[3]

[1]Bremen University, MARUM, Center for Marine Environmental Sciences (Germany);

[2]School of Ocean and Earth Science, University of Southampton, European Way, SO14 3ZH, Southampton (UK);

[3]Department of Earth Sciences, University College London, London (UK);

[4]Laboratoire des Sciences du Climat et de l'Environnement (LSCE/IPSL), Université Paris-Saclay, Gif-sur-Yvette (France).

[5]School of Earth and Environmental Sciences, Cardiff University, Cardiff (UK)

*Corresponding author: Flavia@uni-bremen.de,

d.evans@soton.ac.uk, mawbeye@gmail.com, william.gray@lsce.ipsl.fr, p.pearson@ucl.ac.uk,

b.wade@ucl.ac.uk

Abstract

The ratio of the trace element Mg over Ca (Mg/Ca) and the oxygen isotopic composition (δ^{18}O) of foraminiferal calcite are widely employed for reconstructing past ocean temperatures, although geochemical signals are also influenced by several other factors that vary temporally and spatially. Here, we analyze a global dataset of Mg/Ca and δ^{18}O data of 59 middle Miocene to Holocene species of planktonic foraminifera from a wide range of depth habitats, many of which have never been analyzed before for Mg/Ca. We investigate the extent to which Mg/Ca and δ^{18}O covary through time and space, and identify several sources of mismatch between the two proxies. Once the data are adjusted for long term non-thermal factors, Mg/Ca and δ^{18}O are overall positively correlated in a way consistent with temperature being the dominant controller both through space and time and across many different species, including deep-dwellers. However, we identify several species with systematic offsets in Mg/Ca values, to which multispecies calibrations should be applied with caution. We can track the appearance of such offsets through ancestor-descendent species over the last 15 million years and propose that the emergence of these offsets may be the

27 geochemical expression of evolutionary innovations. We find virtually all of the Mg/Ca and δ^{18}O-

28 derived temperatures from the commonly used genera *Globigerinoides* and *Trilobatus* are within

29 uncertainty of each other, highlighting the utility of these species for paleoceanographic

30 reconstructions. Our results highlight the potential of leveraging information from species lineages

31 to improve sea surface temperature reconstruction from planktonic foraminifera over the

32 Cenozoic.

33 **1. Introduction**

34 Geochemical analyses of foraminifera are commonly applied to reconstruct paleoceanographic

35 conditions, such as marine temperatures, and therefore infer past climatic changes. In particular,

36 the fossil tests of planktonic foraminifera (calcareous zooplankton) provide one of the most widely

37 used paleoclimate archives. Here we focus on two of these parameters: δ^{18}O and Mg/Ca, both of

38 which have been used widely as temperature proxies.

39 The oldest and possibly most widely utilized of these proxies is the ratio of oxygen isotopes in

40 their calcite test which, due to slight differences in reactivity of molecules containing the different

41 isotopes, is temperature-dependent (Urey, 1947; see Pearson, 2012 for review). This effect has

42 been quantified in experiments with inorganic calcite (e.g., Kim and O'Neill, 1997) and planktonic

43 foraminifera in culture (e.g., Erez and Luz, 1983; Bemis et al., 1998). Tests of planktonic

44 foraminifera calcifying in warmer waters are depleted in ^{18}O relative to species living in cooler

45 waters (Emiliani, 1954). A second, more recently established paleoclimate proxy is the ratio of

46 magnesium to calcium in test calcite (Chave 1954; Nürnberg et al., 1996). During inorganic

47 precipitation experiments, the Mg/Ca ratios of calcite were found to be higher at greater

48 temperatures (Mucci, 1987). This relationship led to the in-depth exploration of Mg/Ca ratios in

49   planktonic and benthic foraminifera and its potential application as a temperature proxy through

50   culturing (Lea et al., 1999; von Langen et al., 2005), core top (Nürnberg, 1995; Elderfield and

51   Gassen, 2000) and sediment trap studies (Anand et al., 2003).

52   As they represent two different chemical systems, the Mg/Ca and oxygen stable isotope ratios in

53   foraminifera are often used together as independent temperature proxies. For instance, $\delta^{18}O$

54   derived calcification temperatures have been combined with Mg/Ca data to derive Mg/Ca

55   temperature calibrations (e.g., Anand et al., 2003; McConnel and Thunell, 2005; Mohtadi et al.,

56   2009). Other studies have applied these two systems together to infer the influence of

57   environmental parameters such as seawater salinity on Mg/Ca (e.g., Mathien-Blard and Bassinot,

58   2009; Hönisch et al., 2013) and global ice volume (e.g., Lear et al., 2000; Katz et al., 2008). Works

59   such as these assume covariance of the two proxies for any given sample, which should be the case

60   if both systems are impacted purely by calcification temperature. Nonetheless, there are known

61   non-thermal effects influencing both Mg/Ca and $\delta^{18}O$. For oxygen isotope values, these include

62   the oxygen isotopic composition of seawater ($\delta^{18}O_{sw}$) and to a lesser degree, seawater pH or

63   carbonate ion concentration (Spero et al., 1997; Zeebe, 1999). Seawater carbonate chemistry has

64   also been shown to impact the Mg/Ca proxy. Culture and sediment trap studies demonstrate surface

65   ocean seawater pH can influence Mg/Ca in planktonic foraminifera (Lea et al 1999; Evans et al.,

66   2016a; Gray et al 2018), with the sensitivity of Mg/Ca to pH appearing to vary between species

67   (Gray and Evans 2019). Mg/Ca values of foraminifera are also dependent on the Mg/Ca of

68   seawater (Evans et al., 2016b), and both oxygen isotope and Mg/Ca values can be impacted by test

69   recrystallization (Dekens et al., 2002). Mg/Ca values are susceptible to the preferential loss of Mg

70   during dissolution, and are thus influenced by the calcite saturation state of bottom waters

71   (Regenberg et al 2014; Tierney et al 2019). Seawater salinity has a minor secondary effect on

72 Mg/Ca values (Kisakürek et al., 2008, Hönisch et al., 2013) and whilst salinity has little direct

73 effect on oxygen isotopes, a change in salinity is usually accompanied by a change in $\delta^{18}O_{sw}$

74 because hydrological processes such as evaporation and precipitation are closely coupled

75 (LeGrande and Schmidt 2006). Lastly, so-called 'vital effects', which lump together a wide variety

76 of species-specific processes such as metabolism (including the process of calcification and the

77 incorporation of metabolic products), the position within the water column and life cycle depth

78 migration, the presence of photosymbionts, and seasonality (see summary in Schiebel and

79 Hemleben, 2017), also add complexity to the interpretation of both the oxygen isotope and Mg/Ca

80 proxies.

81 Here we use the dataset published in Boscolo-Galazzo, Crichton et al., (2021), to examine

82 covariance between Mg/Ca and $\delta^{18}O$ in planktonic foraminifera extracted from sediments across

83 a wide range of geographic locations, time intervals, and species. The dataset is composed of $\delta^{18}O$

84 and Mg/Ca data measured on 59 species of planktonic foraminifera, of which 24 have never before

85 been measured for Mg/Ca (Supplementary Tables 1, 2). The data are from different ocean basins

86 and latitudes and a range of ages between the middle Miocene (~15 million years ago, Ma) and

87 the Holocene. Paired Mg/Ca and $\delta^{18}O$ were measured on the same samples, hence this dataset is

88 ideally suited to isolate potential ecological, environmental and preservational factors which may

89 imprint Mg/Ca or $\delta^{18}O$ or both, and which are otherwise impossible to recognize in studies

90 focusing on a limited number of species, a narrow study area or time interval. In particular, it

91 provides the unique opportunity to simultaneously: (1) compare coupled $\delta^{18}O$ and Mg/Ca data on

92 a broader than usual geographical and temporal scale; (2) Compare coupled $\delta^{18}O$ and Mg/Ca data

93 across species of different ecologies; (3) Evaluate Mg/Ca data of extinct species against those of

94 their modern descendants; (4) Test whether temperature can still be recognized as predominantly

95   driving covariance in the dataset when spatial, temporal and ecological variables are

96   simultaneously in play.

2. Material and Analytical methods

98   2.1 Material

99   The dataset (Boscolo-Galazzo, Crichton et al., 2021) was produced from a range of globally and

100   latitudinally distributed DSDP (Deep Sea Drilling Program), ODP (Ocean Drilling Program), and

101   IODP (Integrated Ocean Drilling Program/International Ocean Discovery Program) sites (Fig. 1)

102   which are high in carbonate and composed of calcareous nannofossils and foraminiferal pelagic

103   oozes, with some input of siliceous plankton. Sites were selected based on the best available global

104   and temporal coverage and preservation of foraminifera. Planktonic foraminiferal preservation

105   ranges from excellent to very good (recrystallized but lacking overgrowth and infilling) (Boscolo-

106   Galazzo, Crichton et al., 2021) with the exception of Sites U1490 and U1489, where there is some

107   overgrowth and infilling in the middle Miocene (Fayolle and Wade, 2020; Boscolo-Galazzo,

108   Crichton et al., 2021). The target time intervals selected for sampling were 0, 2.5, 4.5, 7.5, 10, 12.5

109   and 15 Ma. Biostratigraphic analysis was used to assess age using the biochronology of Wade et

110   al. (2011) calibrated to the time scale of Lourens et al. (2004) (Supplementary Table 1).

111   2.2 Planktonic foraminifera

112   Fifty-nine species of planktonic foraminifera were analysed for Mg/Ca and $\delta^{18}O$. Planktonic

113   foraminiferal were picked from three constrained size fractions: 180-250 µm, 250-300 µm and

114   300-355 µm. Planktonic foraminiferal geochemistry can change through size (e.g., Birch et al.,

115   2013), so here we used data from the size fraction 250-355 µm only, giving a total of 57 species

116   in the dataset. For abundant species, up to 80 specimens were picked for geochemical analysis,

117 with as many as possible picked in the case of less common species. Hence, our foraminiferal data

118 represent an average from multiple specimens. Paleodepth habitat attributions follow Boscolo-

119 Galazzo, Crichton et al. (2021) and Boscolo-Galazzo et al. (2022). Planktonic foraminiferal

120 taxonomy follows the concepts described in Boscolo-Galazzo et al. (2022).

121
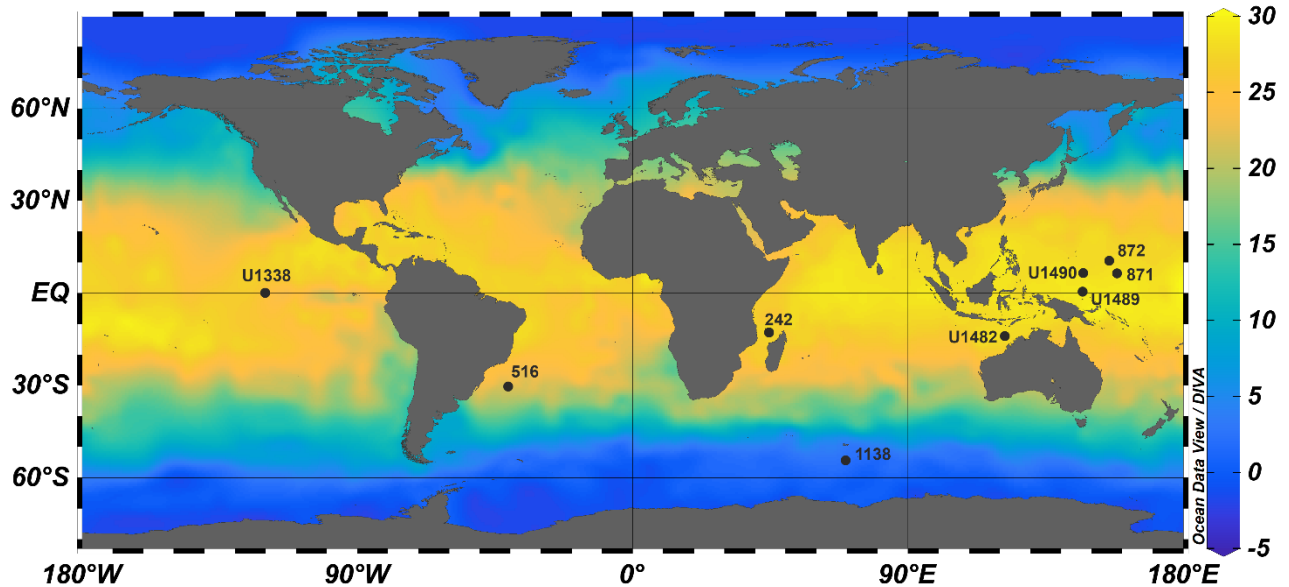
122 **Figure 1.** Site map with present-day mean annual sea surface temperatures (°C) from the World
123 Ocean Atlas 2013 (Locarnini et al., 2013).

124 2.3 Trace element and stable isotope analysis

125 Picked planktonic foraminifera were crushed between two glass slides to open all large chambers.

126 When there was enough material, the crushed sample was split for stable isotope and trace element

127 analysis. The trace element split was cleaned using a protocol to remove clays and organic matter

128 (step A1.1-A1.3 of Barker et al. (2003)). The samples did not undergo reductive cleaning due to

129 their fragility and small sample size, and because the reductive step may cause preferential removal

130 of high Mg/Ca calcite from the test (Yu et al., 2007). Samples were dissolved in trace metal pure

131 0.065 M HNO_3, then diluted with trace metal pure 0.5 M HNO_3 and analysed at Cardiff University

on a Thermo Fisher Scientific Element XR ICP-MS against standards with matched calcium

concentration to reduce matrix effects (Lear et al., 2002). Long term analytical precision

determined from consistency standards (CS1 and CS2) with Mg/Ca ratios of 1.24 mmol/mol and

7.15 mmol/mol are ~0.7 and ~0.8% (relative standard deviation). Mg/Ca was plotted against Fe/Ca

and Mn/Ca to assess whether there was any relationship as a result of the presence of Fe-Mn

oxyhydroxides affecting Mg/Ca, but there was no correlation between the contaminant indicators

and Mg/Ca (Supp. Fig. 1).

Stable isotopes were measured on a Delta V Advantage with Gasbench II mass spectrometer at the

Cardiff University stable isotope facility. Stable isotope results were calibrated to the VPDB scale

using an in-house carbonate standard (Carrara marble). Analytical precision was 0.05‰ for $\delta^{18}O$

and 0.05‰ for $\delta^{13}C$.

2.4 Data analysis

Before performing the analysis, we screened the dataset for outliers, and removed one anomalously

high datapoint with a Mg/Ca value >9 mmol/mol which we attributed to analytical error

(Supplementary Table 1).

2.4.1 Formulation of theoretical relationships between Mg/Ca and $\delta^{18}O$

To test for covariation between Mg/Ca and oxygen isotope data, we regressed the data against each

other and compared the observed relationship with that expected from modern calibrations. We

did this to initially explore the dataset and what kind of relationship we might expect between

Mg/Ca and $\delta^{18}O$ and whether this manifests in the dataset, before applying corrections for the non-

thermal influences on both proxies. Given the complexity of the sample set (e.g., multiple species,

ages, locations, preservation), different expected relationships between Mg/Ca and $\delta^{18}O$ are

154   possible, which depend on: i) species-specific vital effects, ii) the non-thermal controls on Mg/Ca,

155   (salinity, pH, Mg/Ca_{sw}), iii) non-thermal controls on $\delta^{18}O$ ($pH/[CO_3^{2-}]$), $\delta^{18}O_{sw}$, as well as how

156   these factors change through time. To account for this, we calculated a number of possible

157   expected theoretical relationships to give a sense of how much of the scatter in the raw data is

158   likely to be explicable by these factors and inform our following data-analysis accordingly. We

159   stress that this exercise was conducted as a mean of exploring the whole data set; no single

160   relationship will be able to explain the dataset because it is influenced by multiple, often

161   interlinked, variables.

162   Expected theoretical relationships were calculated starting with modern laboratory culture

163   calibrations, onto which the key non-thermal long-term and spatial controls on these proxies were

164   sequentially added to demonstrate how much each of these is expected to shift the slope of the

165   expected Mg/Ca-$\delta^{18}O$ relationship (Fig. 2A). Specifically, we i) combined the Mg/Ca temperature

166   calibrations for *Globigerinoides ruber* and *Trilobatus sacculifer* of Gray & Evans (2019) with the

167      $\delta^{18}O$-temperature equation of Erez & Luz (1983), ii) added the impact of a 0.15 unit whole ocean

168   pH change (approximating the magnitude of the Neogene whole ocean change, e.g., Rae et al.,

169   2021) using the pH-Mg/Ca slope for *G. ruber* as an example (note that this is only applicable to

170   species that show a pH sensitivity) (Evans et al., 2016a), iii) included the expected control of

171   temperature on pH via the T-dependent dissociation of water (K_W), i.e., temperature-driven pH

172   changes within a given time interval independent of whole ocean pH shifts (Gray et al., 2018), iv)

173   showed the impact of Mg/Ca_{sw} half of the modern ratio (Evans et al., 2016b), v) included the effect

174   of pH or $[CO_3^{2-}]$ on $\delta^{18}O$ (Spero et al., 1997; Zeebe, 1999) given the covariance of temperature

175   and pH described in point iii above using the multispecies average slope of Gaskell et al. (2023),

176   and finally vi) explored the likely impact of the covariance of $\delta^{18}O_{sw}$ and temperature that is

177 characteristic of the modern ocean and arises from the broad coupling of the hydrological cycle

178 with surface temperatures. Specifically, this latter influence was calculated by combing SST data

179 from the 2013 World Ocean Atlas (Locarnini et al., 2013) and $\delta^{18}O_{sw}$ from LeGrande & Schmidt

180 (2006), taking all surface ocean data except that from polar meltwater regions, which demonstrates

181 that, on average, in the modern ocean $\delta^{18}O_{sw}$ increases by 0.0425 ‰ per °C SST increase.

182 Each of these factors was applied additively such that (e.g.) the fourth factor listed above

183 (Mg/Ca$_{sw}$) in Fig. 2 includes numbers 1 through 3. The sum of the influence of these factors on

184 the theoretical $\delta^{18}O$-Mg/Ca relationship is represented by the thick blue line in Figure 2A and the

185 black line in Figures 3, 6, 7 and 8, which has a slope of –2.08 in $\delta^{18}O$-ln(Mg/Ca) space.

186 The magnitude of some of these potential non-thermal controls on the two proxies over the time

187 interval studied here are reasonably well constrained. Specifically, the long-term whole ocean pH

188 and Mg/Ca$_{sw}$ changes are sufficiently well known (Rae et al., 2021; Zhou et al., 2021; Brennan et

189 al., 2013) that they can be "subtracted" out of the raw proxy values, given that they are likely to

190 apply to all or most species in the dataset. As such, we next explored the degree to which the

191 Mg/Ca-$\delta^{18}O$ covariation improves once long-term whole ocean pH and Mg/Ca$_{sw}$ changes are

192 removed. To avoid (possibly incorrect) a-priori assumptions regarding, for example, which

193 Mg/Ca-temperature calibration should be applied to each species in the dataset and the degree to

194 which surface ocean $\delta^{18}O_{sw}$ has varied at the study sites, we initially did this keeping the Mg/Ca

195 and $\delta^{18}O$ comparison in raw proxy space and: 1) converted the raw Mg/Ca values to temperature

196 using the multispecies Mg/Ca-temperature calibration from Gray and Evans (2019), together with

197 our best estimate of pH and Mg/Ca$_{sw}$ (as described below (§2.4.2)), and 2) converted the

198 temperatures back into Mg/Ca using the same calibration but modern seawater Mg/Ca and pH.

199 Conceptually, this is equivalent to correcting the raw proxy values for these nonthermal controls.

200   In addition, we subtracted out the long-term whole ocean change in $\delta^{18}O_{sw}$ related to continental

201   ice growth using the sea level curve of Rohling et al. (2022) and a sea level-$\delta^{18}O_{sw}$ scaling factor

202   of 1‰ per 67 m. This results in a raw proxy dataset in which the aforementioned long-term non-

203
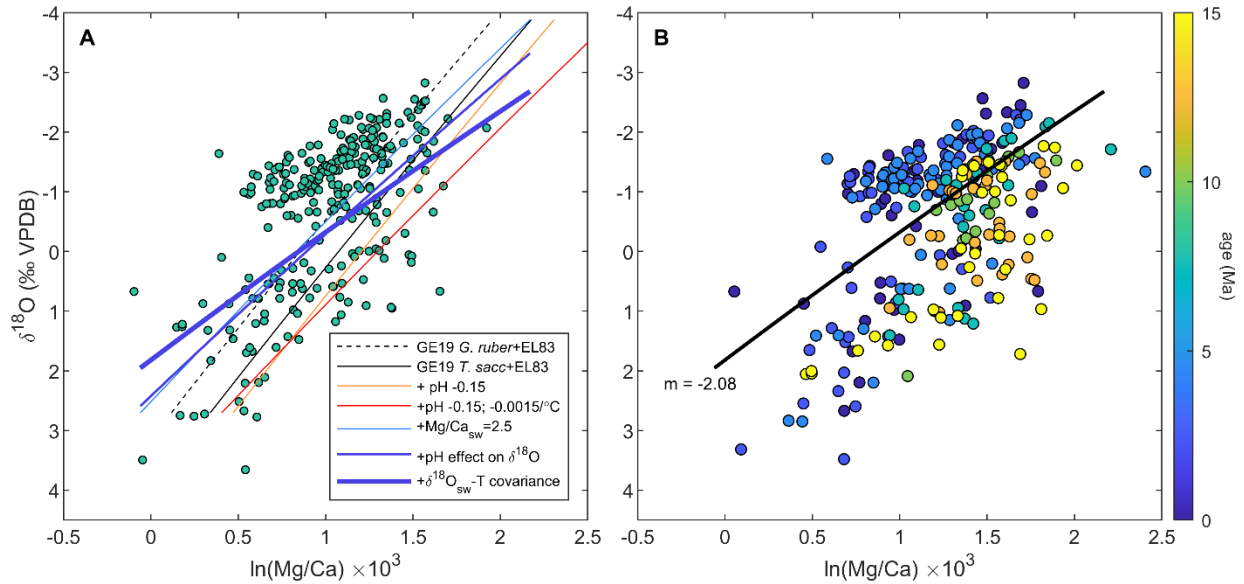
204   **Fig. 2**. Raw $\delta^{18}O$ plotted against Mg/Ca for all samples presented here. (A) Several possible expected
205   Mg/Ca-$\delta^{18}O$ slopes are shown for comparison, including that for *G. ruber* and *T. sacculifer* (at constant pH)
206   in the modern ocean (solid and dashed black lines respectively). The additive impact of nonthermal controls
207   are then explored using the *G. ruber* calibration as an example, specifically, the impact of: a whole-ocean
208   pH shift of 0.15 units (orange line), accounting for the covariation of pH and temperature (driven by the
209   temperature-dependent dissociation of water, red line), seawater Mg/Ca half of the present day value (thin
210   blue line), the theoretical impact of pH on $\delta^{18}O$ (blue line), and the covariance of temperature and $\delta^{18}O_{sw}$ in
211   the modern ocean (thick blue line). We stress that the magnitude of the pH, Mg/Ca$_{sw}$, and $\delta^{18}O_{sw}$ changes
212   applied to these theoretical lines were chosen to illustrate the sensitivity of the two proxies to these factors
213   and do not necessarily represent the degree to which these factors differed in any specific time interval
214   compared to today. The length of each line depicts the expected Mg/Ca and $\delta^{18}O$ change across the same
215   temperature range in each case (5-35°C). All calculations assume $\delta^{18}O_{sw} = 0$‰. (B) As in panel A, except
216   with the long-term whole ocean changes in pH, Mg/Ca$_{sw}$, and $\delta^{18}O_{sw}$ subtracted from the raw proxy values
217   (see text, using the multispecies calibration of Gray & Evans (2019) in the case of the Mg/Ca corrections),
218   i.e., accounting for the impact of these non-thermal Mg/Ca and $\delta^{18}O$ controls. Sample age is shown as a
219   function of colour. Note that the black line is not a regression but rather shows one possible theoretical
220   Mg/Ca-$\delta^{18}O$ relationship and is identical to the thick blue line from panel A including the combined effect
221   of all factors explored there. The slope of this theoretical relationship is -2.08, which provides an
222   approximate expected slope of Miocene-Recent Mg/Ca versus $\delta^{18}O$, although we note that no real-world
223   dataset will conform exactly to this as pH, Mg/Ca$_{sw}$, and $\delta^{18}O_{sw}$ have not (perfectly) covaried through time.

224

225 thermal factors are no longer present and which can be used to evaluate the occurrence of residual

226 scatter independent of the long term non-thermal controls on Mg/Ca and $\delta^{18}O$ (Fig. 2B).

227 2.4.2 Transformation of proxy values into paleotemperature

228 Measured foraminifera Mg/Ca was transformed into paleotemperature using the *MgCaRB* tool

229 (Gray & Evans, 2019; https://github.com/willyrgray/MgCaRB (*R*);

230 https://github.com/dbjevans/MgCaRB (*Matlab*)) which takes into account:

231 - Salinity. Although this has a minor effect on Mg/Ca (Hönisch et al., 2013), whole ocean

232   changes are nonetheless accounted for using a salinity reconstruction derived from scaling

233   the $\delta^{18}O$ benthic stack (Westerhold et al., 2020) to the sea level record of Spratt & Lisiecki

234   (2016), which is then applied to derive sea level between 0.8 and 8 Ma, before which that

235   of Rohling et al. (2022) was used, rescaled to match the $\delta^{18}O$-derived reconstruction at 8

236   Ma and a sea level of +67 m in an ice-free world at 50 Ma. We applied the multispecies

237   salinity sensitivity of Gray & Evans (2019) to all species (3.6% per salinity unit).

238 - pH. Long-term whole ocean changes were derived from a smoothing spline fit to the boron

239   isotope-derived pH data compiled by Rae et al. (2021). We applied species-specific pH-

240   Mg/Ca sensitivities of Gray & Evans (2019) where available for a given species/lineage

241   (discussed in more detail below) and used the multispecies sensitivity in all other cases.

242 - Mg/Ca_{sw} was derived by combining the $[Ca^{2+}_{sw}]$ record of Zhou et al. (2021) with a

243   smoothing spline fit to the fluid inclusion $[Mg^{2+}_{sw}]$ data given in Brennan et al. (2013).

244   Raw Mg/Ca values were adjusted using the equation $Mg/Ca_{corrected} = Mg/Ca_{raw} \times$

245     $Mg/Ca_{sw}^{H}/5.2^{H}$, where $H = 0.64$ based on a data compilation of three foraminifera species

246   and inorganic calcite (Holland et al., 2020; Evans et al., 2015; 2016b; Mucci & Morse,

247   1983).

248 We initially applied a multispecies equation, because the dataset includes a mix of extant and

249 extinct species, some of these never measured for trace elements before (Supplementary Table 2),

250 or lacking an extant/well-calibrated modern relative. Specifically, we used the multispecies

251 Mg/Ca-temperature equation of Gray & Evans (2019) and applied the multispecies pH, salinity,

252 and temperature sensitivities, together with the *Globigerinoides ruber* pre-exponential coefficient

253 (given a Mg/Ca-T relationship of the form Mg/Ca = BeAT in its simplest form) as most of the

254 species for which high quality data exist are known to be characterized by a Mg/Ca-pH sensitivity

255 (Lea et al., 1999; Kisakürek et al., 2008; Evans et al., 2016a).

256 We subsequently applied species-specific calibrations to selected lineages to explore the degree to

257 which scatter in the dataset can be accounted for by taking into account phylogenetic relationships

258 among ancestor-descendent species. Specifically, the *Trilobatus sacculifer* calibration was applied

259 to the *Trilobatus trilobus - Trilobatus sacculifer* lineage, and the *Orbulina universa* calibration

260 was applied to the *Preaorbulina-Orbulina* lineage, both from laboratory culture studies following

261 Gray & Evans (2019). To *Neogloboquadrina* and its descendent lineage *Pulleniatina* we applied

262 a *Neogloboquadrina pachyderma* calibration with the sensitivities (and their uncertainties) of

263 Tierney et al. (2019) (implemented with a re-fit to the dataset following the *MgCaRB* approach,

264 see Supplementary Figure 1). We then evaluate the improvement relative to the multispecies

265 calibration in samples spanning the middle Miocene to modern. The attribution of phylogenetic

266 relationships follows Aze et al. (2011), Spezzaferri et al. (2018), Leckie et al. (2018) and Fabbrini

267 et al. (2021). All uncertainties were fully propagated via Monte Carlo simulation, including those

268 related to: analysis, calibration coefficients (the coefficients that relate Mg/Ca to temperature, pH,

269 and salinity), and the 95% confidence intervals on the salinity, pH, and Mg/Ca$_{sw}$ reconstructions.

270 Specifically, 10^4 random draws of each of these values within their respective uncertainty bounds

271 were used to generate the reported values and 95% CI (2.5th, 50th, and 97.5th percentiles of the

272 resulting dataset). The relative contributions of the various nonthermal factors impacting Mg/Ca-

273 derived temperature are shown in Supplementary Figure 3.

274 The conversion of $\delta^{18}O$ to paleotemperature followed Gaskell et al. (2023) using: the bayfox

275 calibration (Malevich et al., 2019) and the global and local $\delta^{18}O_{sw}$ of Rohling et al. (2022) and

276 Gaskell et al. (2023) respectively. The calculation was performed twice, both with and without a

277 pH/$[CO_3^{2-}]$ effect on $\delta^{18}O$ (the former using the mean planktonic foraminiferal slope of Gaskell et

278 al. (2023) and the $[CO_3^{2-}]$ record of Zeebe & Tyrrell (2019)). We also explored the impact of using

279 a different sea level/deep ocean temperature reconstruction (Miller et al., 2020) on our results,

280 described in the Results Section and shown in Supplementary Figure 2.

281 When evaluating the paleotemperature reconstructions, we define whether or not the two proxy

282 systems agree within uncertainty by determining if the root sum of squares of the two uncertainties

283 is smaller than the temperature difference between the two proxies. We then proceed to identify

284 possible drivers for the data deviating from the expected Mg/Ca and $\delta^{18}O$ relationship by

285 evaluating the age of the sample, regional changes in $\delta^{18}O$ seawater, depth ecology, and possible

286 species-specific offsets.

287 We note that all of the above corrections assume surface ocean conditions, while the dataset

288 contains a number of species that calcify at depth (Boscolo-Galazzo et al., 2021). Given the

289 uncertainties surrounding past changes in vertical pH and $\delta^{18}O_{sw}$ profiles, we do not attempt to

290 account for this in our data analysis but note that this consideration should be borne in mind when

291 interpreting data from deep-dwelling species.

292 **3. Results**

293   Our basic expectation is that higher Mg/Ca should relate to more negative $\delta^{18}O$ values for warmer

294   temperatures, and *vice versa* for colder temperatures. Despite the large number of variables

295   included, the dataset as a whole shows a significant correlation (Fig. 2A; $R^2 = 0.37$, RMSE = 1.01,

296   p <<0.01) between $\delta^{18}O$ and ln(Mg/Ca). Hence, the $\delta^{18}O$-Mg/Ca covariance can be considered a

297   robust feature over the past 15 Myr for the majority of the species analyzed and across the study

298   sites. Nonetheless, there is a high degree of scatter in the data which suggests that the temperature

299   signal which should lead Mg/Ca and $\delta^{18}O$ data to change consistently in opposite directions is

300   affected by other factors. Our exercise of generating theoretical Mg/Ca-$\delta^{18}O$ relationships (Fig.

301   2A), exploring how the relationship between the two proxies might change through space and time,

302   provides a qualitative indication as to whether the scatter can be attributed to long term non-

303   thermal factors generally corrected for when using the $\delta^{18}O$ and Mg/Ca proxies. The substantial

304   differences between these expected relationships suggests that this is likely to be the case (Fig.

305   2A). In particular, Fig. 2A suggests that both a pH effect and Mg/Ca_{sw} changes through time may

306   explain a substantial degree of the variability observed in the dataset compared to the modern

307   relationships (compare the coloured and black lines, see also Supplementary Figure 3).

308   Nonetheless, accounting for these long-term biases alone in the raw dataset does not remove the

309   scatter (Fig. 2B), suggesting the importance of additional factors, such as vital effects and regional

310   variations in $\delta^{18}O_{sw}$. Data converted into temperature, along with 95% confidence intervals, are

311   shown in Figure 3. In this plot 62% of the data points fall within uncertainty, confirming that a

312   high degree of variability in the raw data can be effectively explained and accounted for by

313   correcting for the known spatially and temporally varying non-thermal effects influencing both

314   proxies.

 et al. (2022) (Supplementary Figure 2) would shift our $\delta^{18}O$ temperature reconstructions of +0.5-3.3°C depending on sample age, with the samples from the 7.5 Ma time slice being mostly affected. Whilst the choice of the record to correct for global $\delta^{18}O_{sw}$ exerts a significant control on $\delta^{18}O$-derived temperatures, it has a minor impact both on our long-term dataset overall (compare Fig. 3 with Supplementary Figure 2) and the proportion of proxy data within combined uncertainty, from 62% to 64%.

We find that deep-dwelling and surface-dwelling species fall within uncertainty in terms of the broad degree of agreement between Mg/Ca and $\delta^{18}O$ derived temperatures, hence different depth-habitat ecologies or calcification environments do not represent a systematic source of offset *per se* (Fig. 3B). Indeed, all the species displaying a temperature offset between the two proxies are surface-dwellers (0-200 m depth, Boscolo-Galazzo et al., 2022), with deep-dwellers characterized by inter-proxy agreement in almost all cases (Fig. 3B). Additional explanations are required for those temperature reconstructions that, all non-thermal and spatial controls included, still plot outside their propagated error uncertainty. The data points outside the combined proxy uncertainties either display >5° C warmer (colder) $\delta^{18}O$ (Mg/Ca) temperatures (upper left area of the plot) or >5°C warmer (colder) Mg/Ca ($\delta^{18}O$) temperatures (bottom right area of the plot) (Fig. 3).
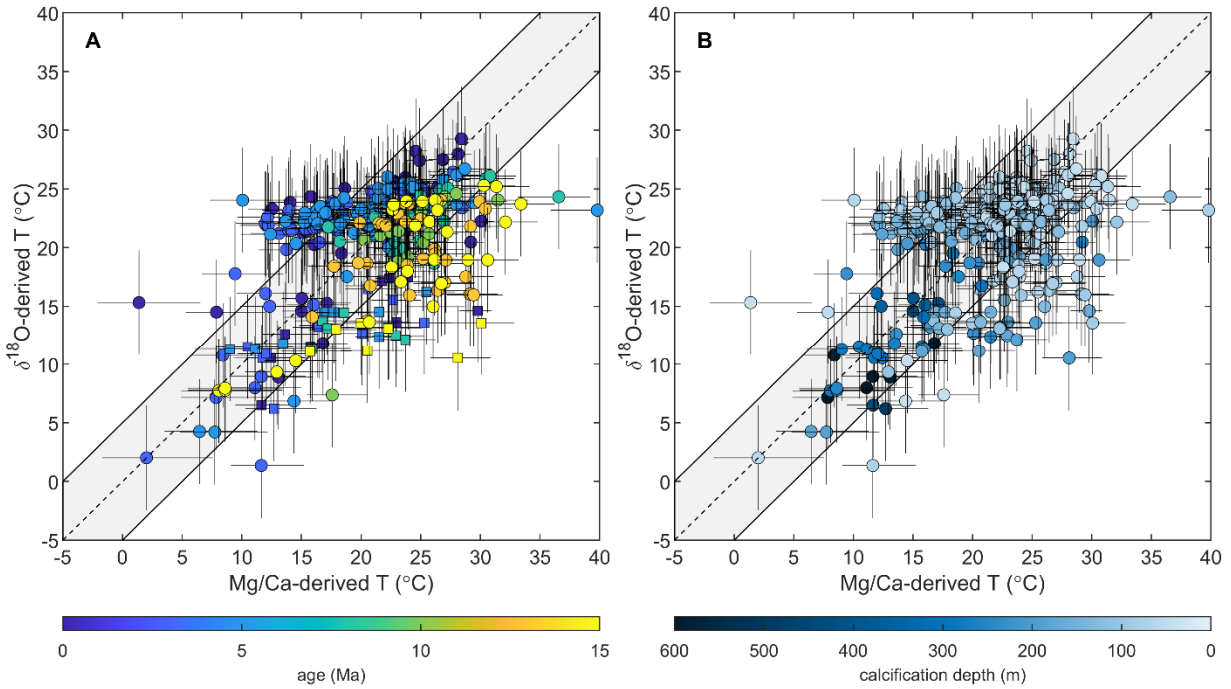
Fig. 3. $\delta^{18}O$ versus Mg/Ca-derived paleotemperatures plotted as function of age (A) and calcification depth (B), accounting for the impact of whole ocean and regional changes in $\delta^{18}O_{sw}$ following Gaskell *et al.* (2022) and the bayfox $\delta^{18}O$-temperature calibration (Malevich *et al.*, 2019), whole ocean changes in Mg/Ca$_{sw}$ and pH on Mg/Ca using *MgCaRB* (Gray & Evans, 2019), and including a pH correction on $\delta^{18}O$ using the mean planktonic foraminifera slope (Gaskell *et al.*, 2023). Fully propagated uncertainties in both proxies are shown, incorporating analysis, calibration, pH, Mg/Ca$_{sw}$, $\delta^{18}O_{sw}$/salinity (see text for details). Site 516 data are shown with square symbols in panel A.

Figure 3A clearly shows that the large majority of the outliers in the upper left part of the plot (warmer $\delta^{18}O$ temperatures or cooler Mg/Ca temperatures) are species of late Miocene to modern age, while the outliers in the bottom right part of the plot (warmer Mg/Ca temperatures) are mostly older species of middle Miocene age or from mid-latitude Site 516 (squares in Fig. 3C). We suggest and discuss possible main sources for these offsets between Mg/Ca and $\delta^{18}O$ temperatures in detail below.

4. Discussion

4.1 Diagenesis

352 Diagenesis is known to alter the test chemistry of foraminifera in three main ways: partial

353 dissolution, overgrowth, and recrystallization (Edgar et al., 2015). The trace element and isotopic

354 composition of tests react differently to these diagenetic processes. The trace element composition

355 of foraminiferal calcite may be susceptible to partial dissolution because it is inhomogeneous

356 (Fehrenbacher et al., 2014), which decreases trace element ratios in species with high and low-Mg

357 regions (Dekens et al., 2002; Edgar et al., 2015; Rongstad et al., 2017), resulting in lower

358 temperature reconstructions. Overgrowth and recrystallization have been shown to add both low-

359 Mg and high-Mg diagenetic calcite, potentially impacting the original signal in opposite directions

360 (Branson et al., 2015), although Mg/Ca is relatively robust to this type of diagenesis, at least in

361 certain circumstances (Staudigel et al., 2022). The oxygen isotopic composition of planktonic

362 foraminiferal tests is well known to be very sensitive to overgrowth and recrystallization (e.g.

363 Sexton et al., 2006), whereby the addition of diagenetic calcite, or the replacement of the original

364 calcite with diagenetic calcite precipitated at the seafloor, can significantly alter the original

365 isotopic signal shifting it to more positive values (Pearson, 2012; Edgar et al., 2015).

366 The Boscolo-Galazzo, Crichton et al. (2021) dataset spans 15 million years and includes sites with

367 different average preservation of foraminiferal tests and oceanographic settings. When the data are

368 regressed against each other (Fig. 2B), we find a total of 26 data points characterized by oxygen

369 isotope values more positive than expected from their Mg/Ca values (Fig. 2B; Supplementary

370 Table 1), resulting in $\delta^{18}O$ temperatures >5° C colder than Mg/Ca temperatures (outside the error

371 envelope) (Fig. 3; Supplementary Table 1). Twenty-one of these data points were from the older

372 time slices (12.5 and 15 Ma), one from the 7.5 Ma time slice and four from the core-top of Site

373 U1338 (Supplementary Table 1).

374   As the majority of these data points were characterized by Mg/Ca values of ~1.5-2 ln(Mg/Ca) (Fig.

375   2B), this yielding more reasonable Mg/Ca than $\delta^{18}O$ temperatures for these sites/time intervals

376   (Supplementary Table 1), the observed offset is most likely best attributed to diagenetic

377   overgrowth/recrystallization, shifting oxygen isotopes towards more positive values without

378   affecting Mg/Ca to the same extent. A recent study compared typical Mg/Ca-$\delta^{18}O$ from

379   recrystallized planktonic foraminifera with chemical diffusive models simulating early diagenetic

380   processes in calcite (Staudigel et al., 2022). According to that study, in a closed system, the bulk

381      $\delta^{18}O$ value will be altered faster than the Mg/Ca, regardless of what partitioning coefficient is used

382   for Mg, leading to a progressive shift to more positive $\delta^{18}O$ values leaving Mg/Ca virtually

383   unchanged (Staudigel et al., 2022).

384   The datapoints presenting $\delta^{18}O$ overprinted by overgrowth/recrystallization were distributed

385   across most of the study sites (except for Sites 871/872), but they were more common at Site

386   U1490 and U1489 (15/26) which are characterized by inferior preservation compared to the others

387   (Boscolo-Galazzo, Crichton et al., 2021). The core-top samples at Site U1338 show clear signs of

388   dissolution with highly fragmented tests. These data points presented the lowest Mg/Ca values in

389   the dataset (1.68 and 0.91 mmol/mol) with temperatures from Mg/Ca lower than from $\delta^{18}O$. This

390   suggests that partial dissolution and recrystallization affected both Mg/Ca and $\delta^{18}O$ in this sample,

391   but Mg/Ca more so.

392   Overall, our scrutiny for diagenesis of the Boscolo-Galazzo, Crichton et al., (2021) dataset is

393   consistent with previous studies suggesting that $\delta^{18}O$ values are more easily affected by

394   recrystallization than Mg/Ca (Sexton et al., 2006; Staudigel et al., 2022; John et al., 2023), similar

395   to other trace element systems (Edgar et al., 2015).

396   Based on the considerations above we excluded the affected 26 data points from the subsequent

397   analysis as being characterized by a stronger diagenetic overprint than the rest of the dataset

398   (Supplementary Table 1). Removing the affected data points in some but not all the cases equated

399   to removing a whole sample (Supplementary Table 1). This is because of variable diagenetically

400   offset $\delta^{18}O$ values from different species in a sample, as observed elsewhere (Sexton et al., 2006;

401   Edgar et al., 2015). The approach used here to reconstruct $\delta^{18}O$ temperature shows that for the

402   majority of the study dataset a diagenetic offset would be comprised within the propagated error

403   envelope (~2-2.5°C) (Fig. 3) and comparable or not distinguishable from an offset deriving from

404   poorly constrained $\delta^{18}O_{sw}$.

405   4.2 Regional scale spatial heterogeneity in seawater chemistry

406   Once converted into temperatures the dataset shows an overall good agreement of Mg/Ca-$\delta^{18}O$

407   data, consistent with temperature being a dominant controller of both proxies through time and

408   across the broad geographical area investigated (Fig. 3). This suggests that, by and large, the

409   seawater corrections applied for the local and global changes in ocean chemistry are adequate,

410   although for one site this may not hold true. Site 516 is a mid-latitude site (south-west Atlantic,

411   30°S) characterized by a modern sea surface temperature around 20°C (Fig. 1), most of the data

412   points from this site have very positive $\delta^{18}O$ values associated with high Mg/Ca (Fig. 2B;

413   Supplementary Table 1). Once converted, this results in $\delta^{18}O$ temperatures that are too cold (12-

414   17°C) compared to both modern (given long-term warming since the Miocene is not expected at

415   any of these sites) and the equivalent Mg/Ca temperatures from the same samples, which are

416   around 21-25°C (Fig. 3A; Supplementary Table 1). We do not attribute this mismatch to diagenesis

417   for a number of reasons. First, Site 516 is characterized by a very good test preservation, much

418   better than at Site U1489 and U1490 for which diagenesis extensively affects the middle Miocene

419   samples; second, this mismatch is observed in the entire dataset through samples spanning the

420   middle Miocene to modern; third, the mismatch is observed for surface-dwelling species only,

421   with deep-dwellers characterised by $\delta^{18}O$ - Mg/Ca in good agreement. Because of its location, Site

422   516 is situated in an area of complex surface hydrography, as it sits at the confluence between the

423   warm Brazil Western Boundary Current and the cold Falkland (Malvinas) Current spinning off

424   from the Antarctic Circumpolar Current (e.g., Jonkers et al., 2021). Compared to the subtropical

425   gyres, where many of the study samples come from, a large degree of spatial variability of surface

426   water physical-chemical properties can be expected on a seasonal and multiannual scale. As such,

427   we suggest that the mismatch between $\delta^{18}O$ and Mg/Ca observed in surface dwelling species at

428   Site 516 may result from changeable surface water properties from the mixing of two very different

429   water masses creating deviations in pH, salinity and $\delta^{18}O_{sw}$ beyond those that are typical in

430   stratified open ocean environments and that are difficult to correct for. Sites with a changeable

431   hydrography such Site 516, may hence not be ideal for the application of geochemical proxies

432   affected by seawater chemistry, unless changes in seawater chemistry at the site can be

433   reconstructed directly.

434   4.3 Species-specific offsets

435   The third and largest source of mismatch that we consider is the occurrence of species-specific

436   offsets, particularly in Mg/Ca given that, in general, the relative degree of inter-species Mg/Ca

437   variability is greater than for shell oxygen isotope composition. For example, the range of inter-

438   species $\delta^{18}O$ offsets is around 1‰ (<4°C), whereas there may be more than a factor of two

439   difference in Mg/Ca between species for a given temperature (e.g., compare Pearson, 2012; Gray

440   & Evans, 2019, Regenberg et al., 2009; Däeron & Gray, 2023). When regressing the data against

441   each other, we find several species presenting systematically offset Mg/Ca values (e.g., Fig. 2B;

442 Supplementary Table 1) leading to proxy-proxy disagreement (Fig. 3; Supplementary Table 1).

443 The occurrence of such offset Mg/Ca values is not evenly distributed across species, but is shared

444 among related species in both spinose and non-spinose groups (Figs. 4-5; Supplementary Table 1).

445 Specifically, the spinose species *Orbulina universa* (2 out of 5 specimens, 2/5), *O. suturalis* (3/6)

446 and *Praeorbulina glomerosa* (1/1) present high Mg/Ca ratios compared to their $\delta^{18}O$ values and

447 Mg/Ca of other species (Fig. 5E). We also find that *Globigerinella siphonifera* (6/7), *G. calida*

448 (1/1), *G. praesiphonifera* (3/4) and *Globigerina bulloides* (5/6) have offset Mg/Ca-$\delta^{18}O$ values,

449 largely being characterized by higher-than-expected Mg/Ca, although three *G. siphonifera* data

450 points show lower Mg/Ca (Figs. 4, 5K; Supplementary Table 1). Among non-spinose species:

451 *Neogloboquadrina humerosa* (11 out of 12 specimens, 11/12), *N. acostaensis* (3/3), *Pulleniatina*

452 *obliquiloculata* (5/6), *P. praecursor* (3/5), *P. primalis* (4/6), *Sphaeroidinella dehiscens* (4/4), and

453 *Sphaerodinellopsis paenedehiscens* (5/10), display Mg/Ca values lower than expected for their

454 oxygen isotope composition (Figs. 4, 5 G, I; Supplementary Table 1).

455 These results highlight for the first time the occurrence of similarly offset Mg/Ca values for

456 ancestor-descent species belonging to the same lineage as well as for whole new lineages (Figs.

457 4,5).

458
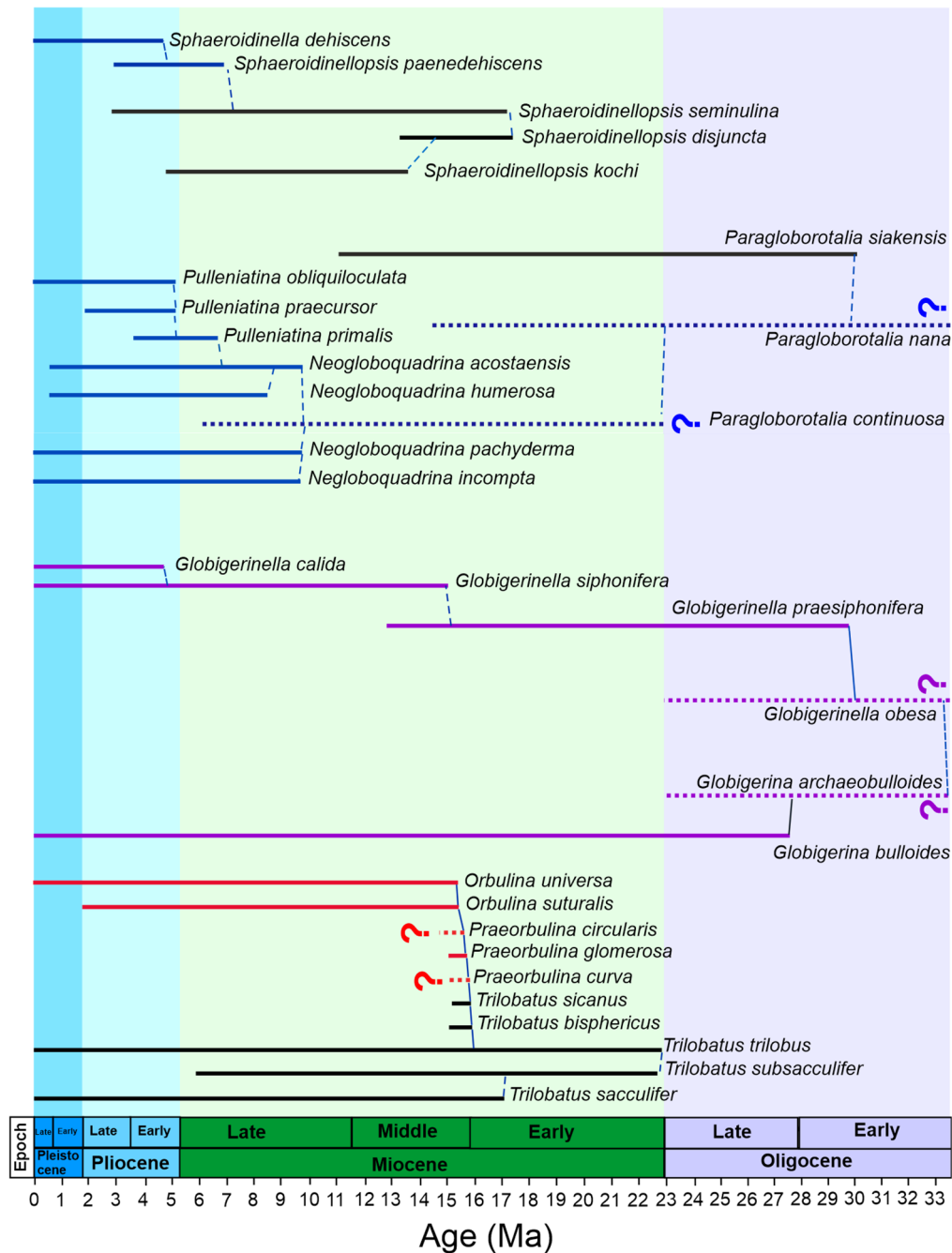
Fig. 4. Phylogenetic relationships of offset spinose and non-spinose species. Shown here are the species discussed in the text, their most closely related species and ancestors. Colored lines indicate species offset in Mg/Ca in the study dataset relative to a multispecies calibration approach, black lines indicate non-offset species. Red lines indicate offset species with higher Mg/Ca, blue lines offset species with lower Mg/Ca, and purple lines species displaying both types of offsets. Question marks indicate the lack of Mg/Ca data for a given species in the dataset presented here. Phylogeny after Aze et al. (2011) and Spezzaferri et al. (2018). The phylogenetic chart was generated using Mikrotax (Huber et al., 2016; www.mikrotax.org/pforams). Ages are from Lourens et al. (2004) for the Neogene and Pälike et al. (2006) for the Oligocene.

468
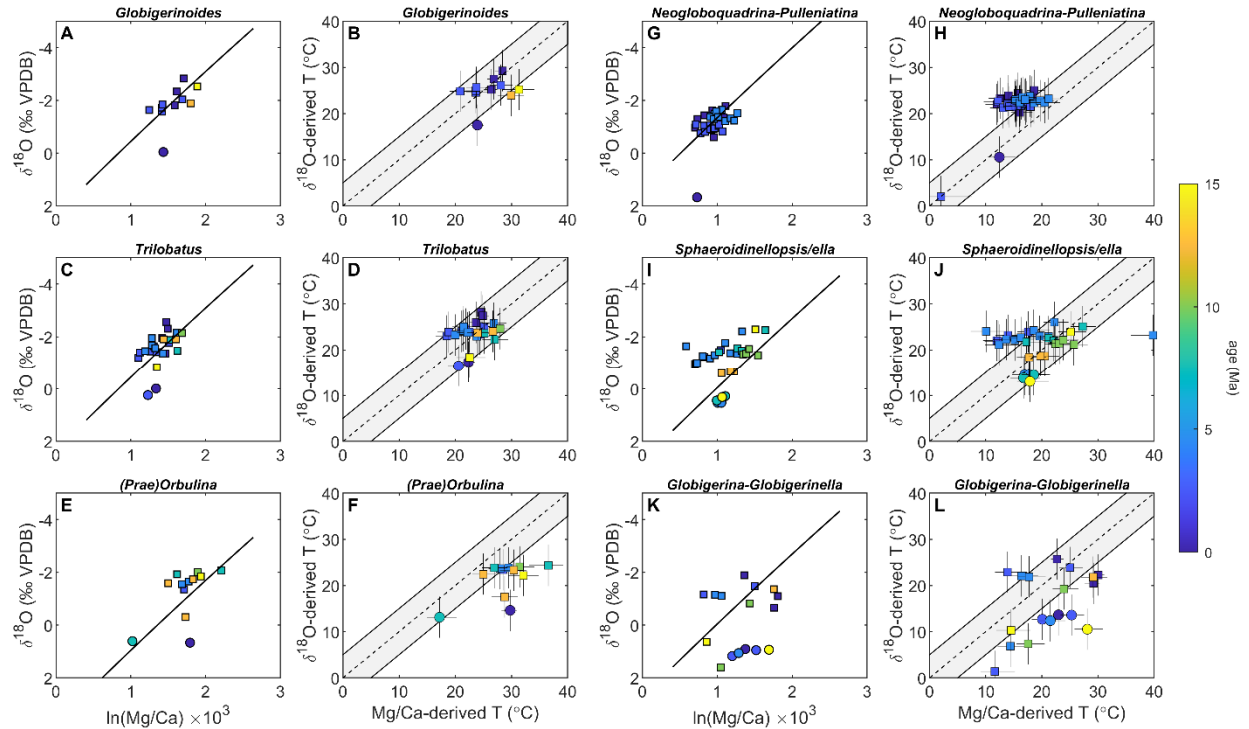
Fig. 5 δ^{18}O versus Mg/Ca and proxy-derived paleotemperature estimates for the ancestor-descendent species *Globigerinoides subquadratus – G. ruber* (panels A and B), *Trilobatus trilobus – T. sacculifer* (panels C and D), *Praeorbulina glomerosa – Orbulina suturalis – O. universa* (panels E and F), *Neogloboquadrina acostaensis – N. humerosa, N. pachyderma – N. incompta, N. acostaensis – Pulleniatina primalis – P. praecursor – P. finalis* (panels G and H), *Sphaerodinellopsis seminulina – S. paenedehiscens – Sphaeroidinella dehiscens, S. seminulina – S. kochi* (panels I and J), *Globigerinella praeshiphonifera – G. siphonifera – G. calida* and *Globigerina bulloides* (panels K and L). Species are defined as offset relative to a multispecies calibration approach when their reconstructed temperature plots outside the gray error envelope (see text for details). Circles indicate data points from Site 516. Raw proxy values are given with the long-term non-thermal controls on Mg/Ca subtracted out (as in Fig. 2), as well as an estimate of paleotemperature (as in Fig. 3). The black lines depict one possible estimate of the expected slope between δ^{18}O and Mg/Ca (the blue line from Fig. 2), adjusted to approximately match the location of the data by shifting them in the direction of δ^{18}O. Datapoints which are considered strongly affected by diagenesis are not included in this plot. Note that one datapoint in panel G falls outside of the plot area.

485

Divergent Mg/Ca values for *G. siphonifera* and *O. universa* have previously been reported (Opdyke and Pearson, 1995; Anand et al., 2003; Friedrich et al., 2012). In the case of *O. universa*, the offset may be related to pH change in the foraminiferal microenvironment due to symbiont

489   photosynthetic activity (Eggins et al., 2004) or changes in seawater pH, with Mg/Ca of the test

490   increasing by as much as 6±3% for each 0.1 unit decrease in pH (Lea et al., 1999; Russell et al.,

491   2004). pH-related vital effects are reported for other spinose species of planktonic foraminifera

492   such as *Globigerina bulloides* (Lea et al., 1999; Davis et al., 2017), which is related to the genus

493   *Globigerinella* (Fig. 4).

494   Among the neogloboquadrinids, *N. acostaensis* and its descendent *N. humerosa* have the most

495   clearly expressed offset with low Mg/Ca values in the study dataset. In contrast, *Neogloboquadrina*

496   *pachyderma* and *N. incompta* are not offset in the study dataset, perhaps simply because of the

497   limited amount of data (one data point each). More broadly, a Mg/Ca offset compared to other

498   species has been reported in the literature (Davis et al., 2017). *Neogloboquadrina dutertrei*, *N.*

499   *incompta*, *N. pachyderma* and *Pulleniatina obliquiloculata* have been shown to be characterized

500   by much lower trace element concentrations (Mg-Ba-Zn/Ca) in the adult portions of their shells

501   (crust and cortex), so that a greater amount of adult versus early ontogenetic calcite leads to low

502   trace element values in bulk shell analysis (Jonkers et al., 2012; Davis et al., 2017; Fritz-Endres &

503   Fehrenbacher, 2021). The low Mg/Ca of crust and cortex have been found to be independent of

504   ambient temperature in cultured *Neogloboquadrina* (Davis et al., 2017) and are found in specimens

505   collected both in surface waters and at depth (Jonkers et al., 2021), indicating that the low Mg/Ca

506   is not acquired due to calcification in deeper, colder waters of the crust/cortex portion of the shell,

507   although a greater incidence of crusts is reported for colder waters (Jonkers et al., 2021). In our

508   dataset, *Neogloboquadrina*, *Pulleniatina* and *Sphaeroidinella/Sphaerodinellopsis* are all

509   characterized by a thick crust or cortex suggesting their Mg/Ca are biased by low Mg adult calcite

510   being quantitatively predominant, which is further corroborated by their Mg/Ca being unrelated to

511 temperature in our data and consistently falling outside of the $\delta^{18}O$-derived temperatures even

512 accounting for the combined uncertainty of the two proxies (Fig. 5 G-H, I-J).

513 The majority of the data points from the offset spinose and non-spinose species results in

514 temperature differences between the two proxies greater than 5°C when using the multi-species

515 calibration from Gray and Evans (2019) as described in §2.4.2, hence outside the calculated error

516 envelope taking all the non-thermal factors discussed above into account (Fig. 5). A similar

517 temperature offset is not apparent for other lineages such *Trilobatus trilobus – Trilobatus*

518 *sacculifer* and *Globigerinoides subquadratus – G. ruber*, to which the same treatment to the offset

519 spinose and non-spinose species was applied (§2.4.2, Fig. 5 A-D). Hence, we attribute the offset

520 temperatures to the atypical Mg/Ca signatures described above in the affected species, in turn

521 resulting from biology/ecology dependent vital effects shared within a lineage and between related

522 lineages (Figs. 4-5).

523 When a species-specific calibration for *Neogloboquadrina pachyderma* is applied to descendent

524 species/lineages and sister taxa (Fig. 6) the offset is successfully corrected for all the

525 *Neogloboquadrina* and *Pulleniatina* species which effectively no longer produce offset

526 temperatures (Fig. 6). *Vice versa*, we only observe a minor improvement when applying the

527 *Orbulina universa* calibration to the *Prearobulina-Orbulina* lineage, with most temperature data

528 points remaining offset (Fig. 6). This may imply that the *O. universa* laboratory calibrations require

529 revision for application to fossil samples. No large difference is observed when applying the

530 *Trilobatus sacculifer* calibration to ancestor-descendent species in the genus *Trilobatus* (Figs. 5-

531 7) although we recommend doing so, given that no Mg/Ca-pH effect is known for this genus, in

532 contrast to (e.g.) *G. ruber*.

533   Overall, this exercise demonstrates that the majority of the data points characterized by proxy-

534   proxy disagreement (Fig. 3) are from the lineages: *Praeorbulina-Orbulina*, *Globigerina-*

535   *Globigerinella, Neogloquadrina-Pulleniatina, Sphaeroidinellopsis-Sphaeroidinella* (Fig. 5). We

536   find that using a "nearest descendant" approach in the choice of temperature calibration improves

537   the agreement between $\delta^{18}O$ and Mg/Ca temperatures for the neogloboquadrinids and

538   pulleniatinids (Fig. 6). At the same time, it enables us to identify "problematic" species and

539   lineages which require further investigations before being used for temperature reconstructions

540   (Fig. 6). Once all the potential sources of offset described above are taken into account, the species-

541   specific calibration for *Neogloboquadrina* is applied, and the data points which are still offset

542   removed from the dataset, the agreement between the two proxies increased from 62 to 91% of

543   data points falling within the combined uncertainties of the proxies (Fig. 7).

544

545

546

547

548

549

550

551

552
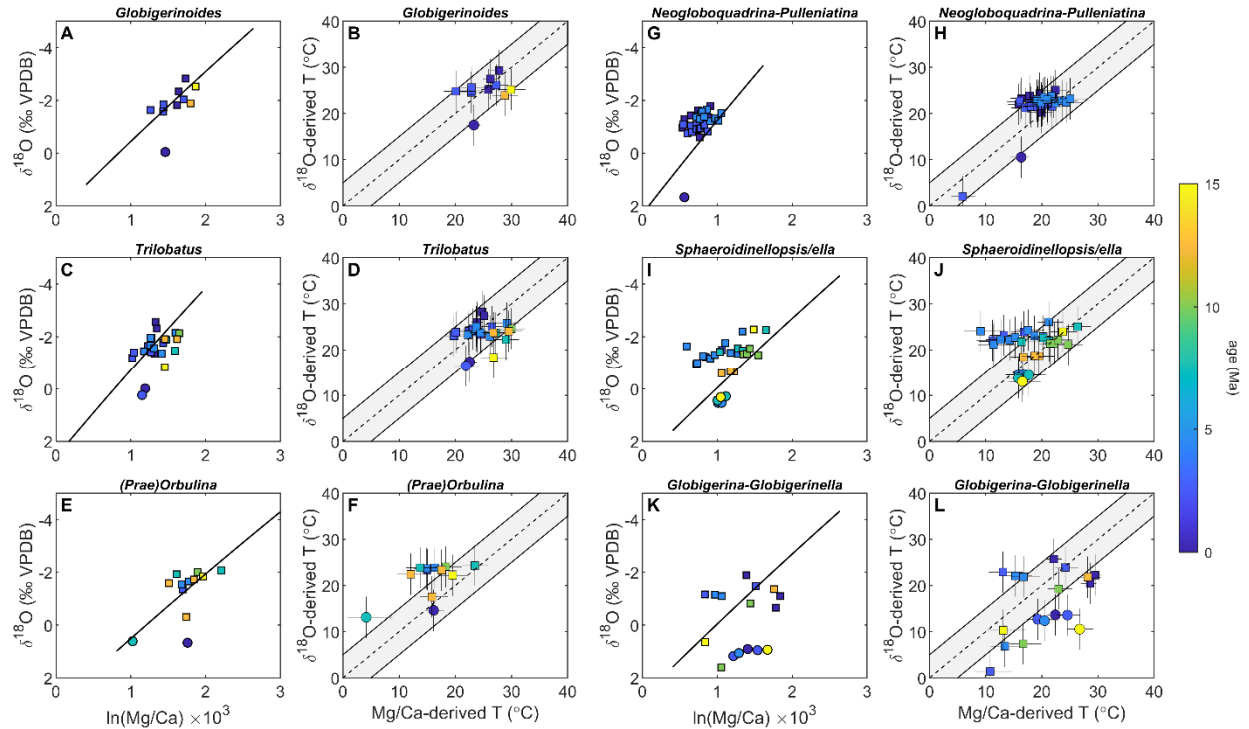
Fig. 6. As in Figure 5, except extending the use of species-specific calibrations to all species in a lineage in the case of the *Trilobatus trilobus – T. sacculifer* (panels C and D), *Praeorbulina glomerosa – Orbulina suturalis – O. universa* (panels E and F), *Neogloboquadrina acostaensis – N. humerosa, N. pachyderma – N. incompta, N. acostaensis* and between related lineages in the case of N*eogloboquadrina* and the *Pulleniatina primalis – P. praecursor – P. finalis* lineage (panels G and H). When applying species-specific calibrations, the offset between Mg/Ca and δ^{18}O temperature is resolved for some species (e.g., all *Neogloboquadrina*, compared to Fig. 5) but not for others, i.e., their reconstructed temperature still plots outside the gray error envelope (e.g., most of *Globigerina* and *Globigerinella*).

562

563
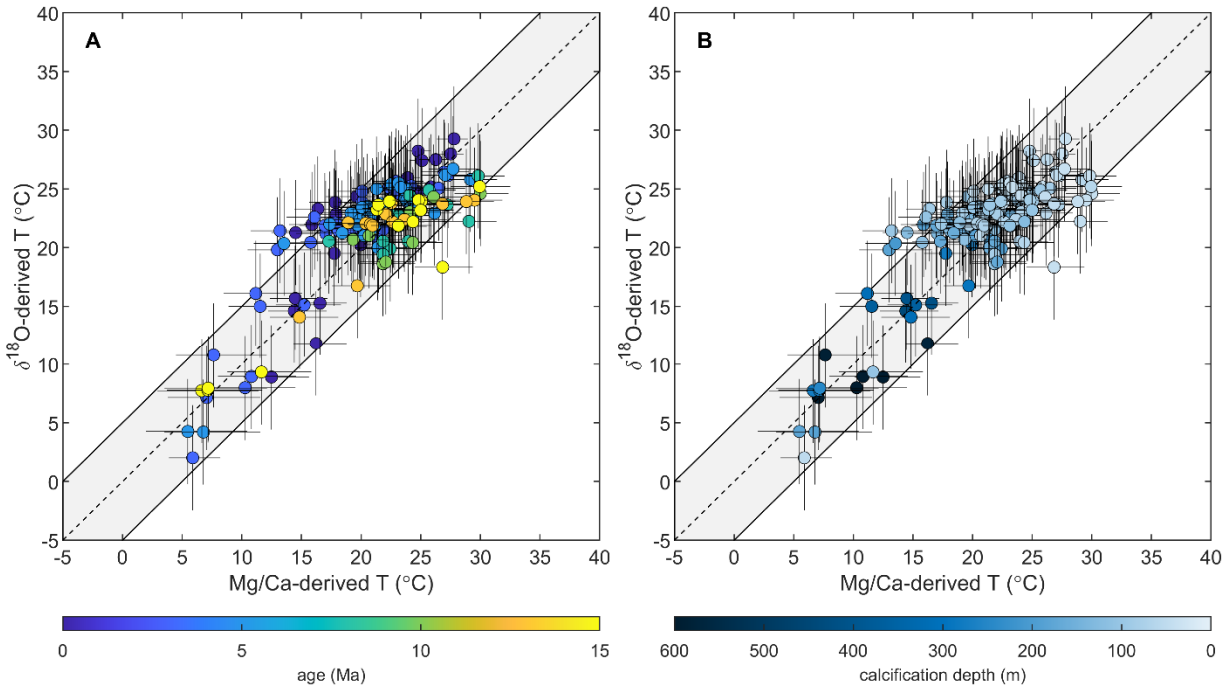
Fig. 7. As Fig. 3, with all offset lineages (§ 4.3; specifically, those that remain offset following the application of lineage-specific calibrations where possible) and diagenetically compromised (§ 3.1) samples removed. Removing these samples leaves 157 data points, of which 92% fall within the combined uncertainty of Mg/Ca-δ^{18}O agreement.

4.4. Planktonic foraminiferal Mg/Ca offsets as an expression of evolution

The analysis of the Boscolo-Galazzo, Crichton et al. (2021) dataset performed here, allows offsets through ancestor-descendent species to be tracked for the first time, and the time of their appearance to be assessed. Specifically, we observe that offsets tend to appear with the origination of a new lineage and to continue to the modern representative(s) of that lineage (Fig. 8). In this way, an attempt can be made to interpret offsets as the geochemical expression of evolutionary new biochemical pathways or ecological strategies in emerging species.

For spinose species, the observed high Mg/Ca offset is shared by ancestor-descendent species such as *Globigerinella praesiphonifera - G. siphonifera* and *Praeorbulina glomerosa - Orbulina*

579 *suturalis - O. universa* (Fig. 4). *Globigerina bulloides* shares the same type of offset with

580 *Globigerinella* and a common ancestor (*Globigerina archaeobulloides*) in the earliest Oligocene

581 (~33.5 Ma) (Spezzaferri et al., 2018) (Fig. 4), suggesting that for this group the offset may go back

582 to at least the early globigerinids of the Paleogene. The genus *Preaorbulina* originated from the

583 genus *Trilobatus* at about 16 Ma (Fig. 4) (Pearson et al., 1997; Aze et al., 2011). *Trilobatus trilobus*

584 is the last common ancestor between the *Trilobatus* and *Prearobulina-Orbulina* lineages (Fig. 4),

585 and does not present offset Mg/Ca-δ^{18}O values, similar to its modern descendants (Figs. 4, 5). This

586 suggests that the offset in *Praeorbulina-Orbulina* originated within the lineage and the

587 morphological changes associated with it (Fig. 8), and carried on to the modern representative *O.*

588 *universa*. Spinose *Globigerinoides ruber* is also reported to be sensitive to pH changes (Kisakürek

589 et al., 2008; Evans et al., 2016b), *G. ruber* is not offset in the analyzed dataset (both in the raw

590 data and calculated temperatures), with ancestor-descendent *G. subquadratus-G. ruber* behaving

591 similarly to the *Trilobatus trilobus – T. sacculifer* lineage through time (Figs. 5, 6), suggesting that

592 this non-thermal effect is adequately accounted for in this case (Fig. 6) (i.e., the laboratory

593 calibration are applicable downcore into deep-time in correcting for this). The on-average higher

594 Mg/Ca displayed by offset spinose *Preaorbulina-Orbulina, Globigerinella* species and *G.*

595 *bulloides* in the study dataset may suggest a lower pH environment which we cannot directly

596 account for (Fig. 2A). For *Globigerina* and *Globigerinella*, where a larger degree of scatter (Fig.

597 6-7 K-L) is observed in association with a rather conservative morphology through time (Fig. 8),

598 the offset may be linked to an opportunistic behavior and capability to adapt to a broad range of

599 environmental conditions with variable pH (Weiner et al., 2015). This may in turn be related to

600 the complexity of genotypes association in both *G. bulloides* and *Globigerinella* species, with

601   different genotypes having different ecologies but almost identical morphologies (e.g., Weiner et

602   al., 2015; Morard et al., 2024).
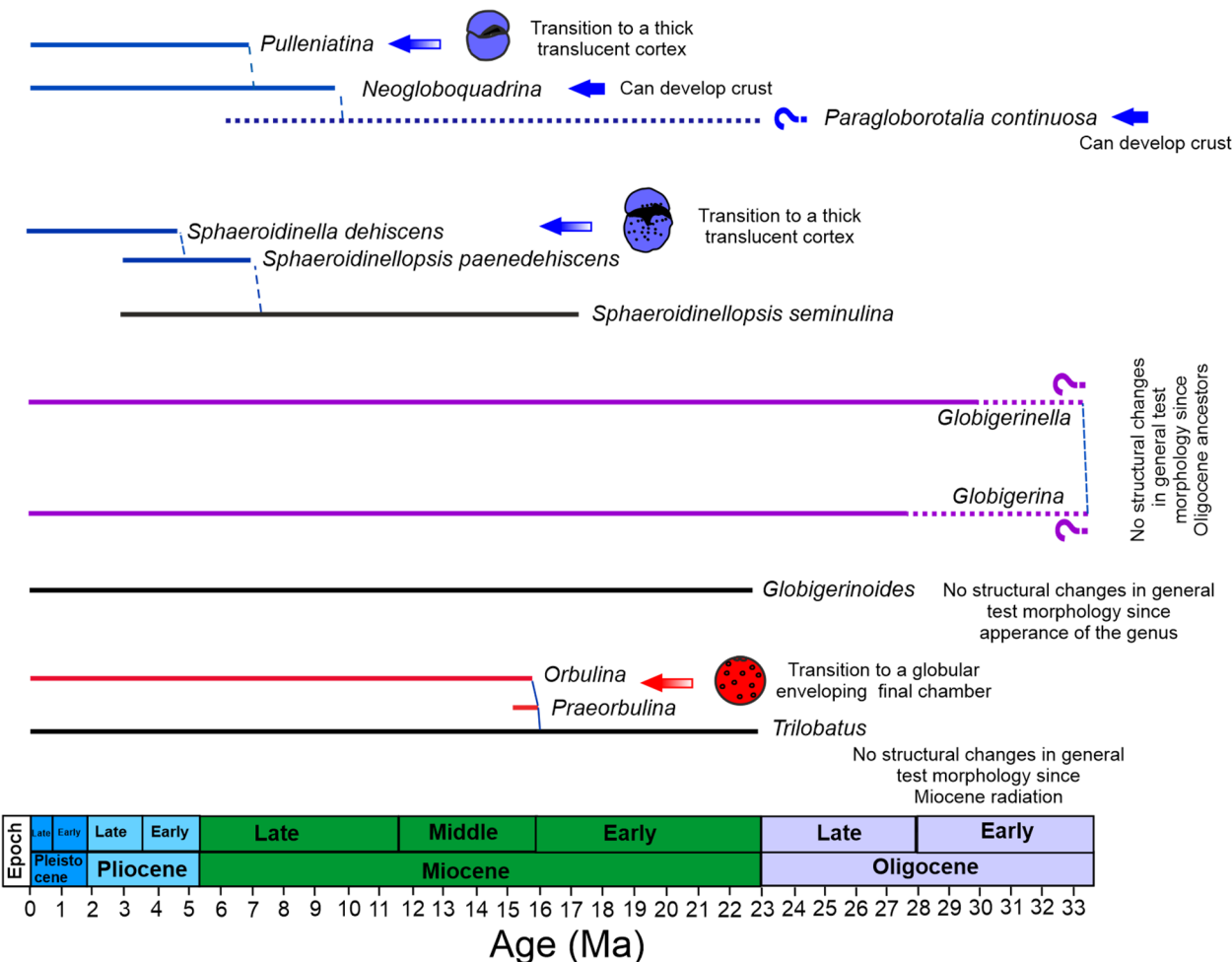
Fig. 8 Simplified phylogeny for the offset lineages discussed in the text with the occurrence of morphological changes associated with their evolution highlighted. Colored lines indicate species offset in Mg/Ca in the study dataset relative to a multispecies calibration approach, black lines indicate non-offset species. Red lines indicate offset species with higher Mg/Ca, blue lines indicate offset species with lower Mg/Ca, and purple lines denote species displaying both types of offsets. Question marks indicate the lack of Mg/Ca data for a given species in the dataset presented here. Phylogeny after Aze et al. (2011) and Spezzaferri et al. (2018). The phylogenetic chart was generated using Mikrotax (Huber et al., 2016; www.mikrotax.org/pforams). Ages are from Lourens et al. (2004) for the Neogene and Pälike et al. (2006) for the Oligocene.

614   We find that the low Mg/Ca offset is shared between ancestor-descendent lineages

615   *Neogloboquadrina-Pulleniatina* and *Sphareoidinellopsis-Sphaerodinella* (Figs. 4, 8).

616 *Neogloboquadrina* evolved from *Paragloborotalia continuosa*, in the late Miocene, at about 10

617 Ma (Fig. 4). While paired Mg/Ca – δ^{18}O measurements for *P. continuosa* are not available, paired

618 Mg/Ca – δ^{18}O measurements for *Paraglobortalia siakensis,* a species older than *P. continuosa,* do

619 not show a low Mg/Ca offset (Supplementary Table 1). This may indicate either that the occurrence

620 of low Mg/Ca crust/cortex started with *P. continuosa*, the youngest representative of the genus

621 *Paragloborotalia* in our study, or with the neogloboquadrinids. The genus *Pulleniatina* evolved

622 from *Neogloboquadrina acostaensis* at about 6.5 Ma (Pearson et al., 2023) (Fig. 4), by modifying

623 the chambers arrangement and progressively developing a cortex (Fig. 8). *Pulleniatina* may have

624 inherited the capability to thicken its test from *Neogloboquadrina* and modified it into a cortex

625 (Fig. 8) (Pearson et al., 2023). The occurrence of a low Mg/Ca cortex in *Pulleniatina* appears to

626 start from the most ancient representative of this group, *P. primalis* (Fig. 4) and continues to the

627 modern. Similar to *Paragloborotalia*, middle Miocene *Sphaeroidinellopsis kochi* and *S.*

628 *seminulina* are not characterized by an offset to low Mg/Ca values (Figs. 4-6). Nonetheless, an

629 offset is observed in 5 out of 10 specimens for late Miocene – early Pliocene S. *paenedehiscens*,

630 and always occurs for its descendent *Sphaeroidinella dehiscens* (Figs. 4-6). Our analysis shows

631 how the occurrence of a low Mg/Ca offset in planktonic foraminifera becomes progressively rarer

632 going back in time, in parallel with the rarity of crust/cortex features (Fig. 8). The occurrence of a

633 crust/cortex is commonly observed in non-spinose modern planktonic foraminifera, however, only

634 two early to middle Miocene genera are known to produce crusts (*Globoconella* and

635 *Paragloborotalia*) and only one is known to produce cortex (*Sphaerodinellopsis*) (e.g., Fig. 8).

636 It is tempting to put the pattern of emergence of Mg/Ca offsets in relationship with changes in

637 ocean chemistry and global climate over the last 15 Myr. In particular, the offset spinose species

638 are mostly tropical and evolved during a time when mean ocean pH was more than 0.1 pH unit

639   lower than preindustrial (Rae et al., 2021). Further, the *Preorbulina - Orbulina* plexus evolved at

640   about 16 Ma (Fig.8), in coincidence with a drop in ocean pH likely linked to the global warmth of

641   the Miocene Climatic Optimum (Rae et al., 2021). The particularly high Mg/Ca signature of this

642   group of species, along with their evolutionary timing, might testify their ability to withstand

643   tropical surface waters more undersaturated than today thanks to changes in the biomineralisation

644   pathway as a consequence of their evolution during the Miocene Climatic Optimum.

645   The evolution of the offset non-spinose species happened several millions of years later during the

646   long-term cooling trend of the last 10 Myr (Fig. 8). The offset species occur across tropical to high

647   latitude areas and mixed-layer (*Sphaeroidinellopsis, Sphaeroidinella*) to intermediate

648   (*Neogloboquadrina, Pulleniatina*) depth habitats. The ability to develop crust/cortex in species

649   evolving over the last 10 Myr might have been of advantage as the global ocean was becoming

650   progressively colder and denser, in a similar way to the observed increases in shell-mass across

651   Pleistocene glacial cycles (e.g., Zarcogiannis et al., 2019).

652   The last 10 Myr were also characterized by decreasing concentration in Ca_{sw} ($[Ca^{2+}]$) in step with

653   global cooling, reaching concentrations half those of the middle Miocene in the Recent (Zhou et

654   al., 2021). Partly as a consequence, Mg/Ca_{sw} doubled over the past 15 Ma (Evans et al., 2016b;

655   Rosenthal et al., 2022). With decreasing $[Ca^{2+}]$ and increasing $[Mg^{2+}]$ in seawater over the

656   Neogene (Brennan et al., 2013; Evans et al., 2016b; Zhou et al., 2021), some species might have

657   started to more actively control the Mg/Ca ratio at their biomineralisation site, e.g., by

658   proportionally decreasing the active transport of Mg^{2+}, in order to buffer against the effects of the

659   higher seawater Mg/Ca, and to keep the outer parts of their shell with low Mg/Ca and thus more

660   resistant to dissolution. Hence, the low Mg/Ca offset observed in the modern and fossils non-

661   spinose species above might be linked to their evolutionary emergence during a time of changing

662   ocean physical-chemical properties, which may have promoted the evolution of thicker tests with

663   a different elemental chemistry making them less buoyant and resistant to dissolution.

5. Conclusions

665   We analyzed a multispecies planktonic foraminiferal $\delta^{18}O$ and Mg/Ca dataset spanning the last 15

666   million years at multiple locations to test whether temperature is the main controller of both proxies

667   and assess the major overprinting factors through time, space and for species with very distinct

668   ecologies. Once diagenesis and possible regional hydrographic factors are taken into account, we

669   find that species-specific offsets not accounted for in our calibration strategy remain a source of

670   mismatch between the two proxies. Specifically, *Globigerina*, *Globigerinella*, *Praeorbulina* and

671   *Orbulina* species are consistently offset, with Mg/Ca values on average higher than expected.

672   Conversely, non-spinose *Neogloboquadrina*, *Pulleniatina*, *Sphaeroidinellpsis* and

673   *Sphaeroidinella* appear consistently offset with low Mg/Ca. The appearance of these geochemical

674   offsets appears to be linked to the origination of new clades, and is shared between ancestor-

675   descendent species, such that we were able to track their evolutionary history. The variable offset

676   in *Globigerinella* may go back to the early globigerinids of the Paleogene and could be related to

677   the opportunistic behavior of this group and emergence of multiple genotypes through geological

678   time, leading to a wider-range of habitat conditions. The high Mg/Ca offset in *Orbulina* starts with

679   *Praeorbulina* in the middle Miocene, while a low Mg/Ca offset appears typical of groups evolving

680   in the late Neogene characterized by a crust or cortex. This pattern suggests that the offsets

681   observed in modern species may be a legacy of their parent groups originating millions of years

682   ago, when ocean properties were different from today.

683 Overall, our study highlights the power of the multispecies and multi-time slice dataset presented

684 here, enabling us to identify the evolutionary origin and timing of deviations in Mg/Ca-

685 temperature/pH relationships. Furthermore, our study demonstrates the robustness of Mg/Ca and

686 $\delta^{18}O$ proxies through geologic time when nonthermal factors (especially Mg/Ca_{sw} and pH) are

687 accounted for. For example, virtually all *Globigerinoides* and *Trilobatus* Mg/Ca and $\delta^{18}O$-derived

688 temperatures are within uncertainty of each other, highlighting the utility of these species for

689 paleoceanographic reconstruction. In addition, our analysis enables us to identify species/lineages

690 that should be treated with caution when interpreting Mg/Ca data, at the very least demonstrating

691 that care should be taken in selecting the calibration approach and highlighting the need for further

692 work in understanding the nonthermal controls on Mg incorporation into the shells of these

693 foraminifera.

694 **Code and Data availability**

695 All data are available as supplementary material of this paper. R and Matlab code to perform the

696 'MgCaRB' protocols are available on Github: https://github.com/willyrgray/ MgCaRB for R,

697 https://github.com/dbjevans/MgCaRB/releases/tag/v1.3

698 for Matlab.

699 **Author contributions**

700 E.M.M. performed trace element analysis; F.B.G conceptualized the paper; D.E. performed data

701 analysis; F.B.G and D.E. produced the figures; F.B.G and D.E. wrote the paper with contributions

702 from all authors.

703 **Competing interests**

704   The authors declare no competing interests.

705   **Acknowledgments**

706   This study was funded by Natural Environment Research Council (NERC) grant NE/N001621/1

707   to P.N.P. (F.B.G.); NERC grant NE/P016375/1 to participate in IODP Expedition 363 (P.N.P.);

708   and NERC grant NE/N002598/1 to B.S.W. (E.M.M.). Marcin Latas assisted with sample

709   preparation funded by an EU Marie Curie Career Integration Grant 293741 to B.S.W; F.B.G

710   acknowledges support from Horizon 2020 Framework Programme (H2020-MSCA-IF-2020

711   101019438).

712   **References**

713   1. Anand, P., Elderfield, H., and Conte, M.H.: Calibration of Mg/Ca thermometry in

714   planktonic foraminifera from a sediment trap time series, Paleoceanography 18, 1050,

715   10.1029/2002PA000846, 2003.

716   2. Aze, T., Ezard, T.H.G., Purvis, A., Coxall, H.K., Stewart, D.R.M., Wade, B.S., and

717   Pearson, P.N.: A phylogeny of Cenozoic macroperforate planktonic foraminifera from

718   fossil data, Biological Reviews 86, 900–927, 10.1111/j.1469-185X.2011.00178, 2011.

719   3. Barker, S., Greaves, M., and Elderfield, H.: A study of cleaning procedures used for

720   foraminiferal Mg/Ca paleothermometry, Geochemistry, Geophysics, Geosystems 4,

721   10.1029/2003GC000559, 2003.

722   4. Birch, H., Coxall, H.K., Pearson, P.N., Kroon, D., and O'Regan, M.: Planktonic

723   foraminifera stable isotopes and water column structure: Disentangling ecological signals,

724   Marine Micropaleontology 10, 127–145, 10.1016/j.marmicro.2013.02.002, 2013.

725   5. Boscolo-Galazzo, F., Crichton, K.A., Ridgwell, A., Mawbey, E.M., Wade, B.S., and
726   Pearson P.N.: Temperature controls carbon cycling and biological evolution in the ocean
727   twilight zone, Science, 371, 1148–1152, 10.1126/science.abb6643, 2021.

728   6. Boscolo-Galazzo, F., Jones, A., Dunkley Jones, T., Crichton, K.A., Wade, B.S., and
729   Pearson, P.N.: Late Neogene evolution of modern deep-dwelling plankton,
730   Biogeosciences, 19, 743-762, doi.org/10.5194/bg-19-743-2022, 2022.

731   7. Branson, O., Read, E., Redfern, S. A. T., Rau, C., and Elderfield, H.: Revisiting diagenesis
732   on the Ontong Java Plateau: Evidence for authigenic crust precipitation in *Globorotalia*
733   *tumida*, Paleoceanography 30, 1490–1502, 10.1002/2014PA002759, 2015.

734   8. Brennan, S.T., Lowenstein, T.K., and Cendon, D.I.: The major-ion composition of
735   Cenozoic seawater: the past 36 million years from fluid inclusions in marine halite,
736   American Journal of Science 313, 713–775, doi.org/10.2475/08.2013.01, 2013.

737   9. Burke, K.D., Williams, J.W., Chandler, M.A., Haywood, A.M., Lunt, D.J., and Otto-
738   Bliesner, B.L.: Pliocene and Eocene provide best analogs for near-future climates,
739   Proceedings of the National Academy of Sciences 115, 13288-13293,
740   doi.org/10.1073/pnas.1809600115, 2018.

741   10. Chave, K. E.: Aspects of the biogeochemistry of magnesium 1. Calcareous marine
742   organisms, The Journal of Geology, 62, 266-283, 10.1086/626162, 1954.

743   11. Daëron, M., and Gray, W. R. Revisiting oxygen-18 and clumped isotopes in planktic and
744   benthic foraminifera. Paleoceanography and Paleoclimatology, 38, e2023PA004660, 2023.

745   12. Davis, C.V., Fehrenbacher, J.S., Hill, T.M., Russell, A.D., and Spero, H.J.: Relationships
746   between temperature, pH, and crusting on Mg/Ca ratios in laboratory-grown

747   Neogloboquadrina foraminifera, Paleoceanography 32, 2017PA003111,

748   10.1002/2017PA003111, 2017.

749 13. Dekens, P.S., Lea, D.W., Pak, D.K., and Spero, H.J.: Core top calibration of Mg/Ca in

750   tropical foraminifera: Refining paleotemperature estimation, Geochemistry, Geophysics,

751   Geosystems 3, 1-29, 10.1029/2001GC000200, 2002.

752 14. Edgar, K.M., Anagnostou, E., Pearson, P.N., and Foster, G.L.: Assessing the impact of

753   diagenesis on $\delta^{11}B$, $\delta^{13}C$, $\delta^{18}O$, Sr/Ca and B/Ca values in fossil planktic foraminiferal

754   calcite, Geochimica et Cosmochimica Acta 166, 189–209, 10.1016/j.gca.2015.06.018,

755   2015.

756 15. Eggins S. M., Sadekov A. and De Deckker P.: Modulation and daily banding of Mg/Ca in

757   *Orbulina universa* tests by symbiont photosynthesis and respiration: a complication for

758   seawater thermometry? Earth Planetary Science Letters 225, 411–419,

759   10.1016/j.epsl.2004.06.019, 2004.

760 16. Elderfield, H., and Ganssen, G.: Past temperature and $\delta^{18}O$ of surface ocean waters

761   inferred from foraminiferal Mg/Ca ratios, Nature 405, 442, 10.1038/35013033, 2004.

762 17. Elderfield, H., Yu, J., Anand, P., Kiefer, T., and Nyland, B.: Calibrations for benthic

763   foraminiferal Mg/Ca paleothermometry and the carbonate ion hypothesis, Earth and

764   Planetary Science Letters 250, 633-649, 10.1016/j.epsl.2006.07.041, 2006.

765 18. Emiliani, C.: Depth habitats of some species of pelagic foraminifera as indicated by oxygen

766   isotope ratios, American Journal of Science 252, 149-158, 1954.

767 19. Erez, J., and Luz, B.: Experimental paleotemperature equation for planktonic foraminifera,

768   Geochimica et Cosmochimica Acta 47, 1025 – 1031, 10.1016/0016-7037(83)90232-6,

769   1983.

770   20. Evans D., Erez J., Oron S. and Muller W.: Mg/Ca temperature and seawater-test chemistry

771   relationships in the shallow-dwelling large benthic foraminifera *Operculina ammonoides*,

772   Geochimica and Cosmochimica Acta 148, 325–342, 10.1016/j.gca.2014.09.039, 2015.

773   21. Evans, D., Wade, B.S., Henehan, M., Erez, J., and Müller, W.: Revisiting carbonate

774   chemistry controls on planktic foraminifera Mg/Ca: Implications for sea surface

775   temperature and hydrology shifts over the Paleocene-Eocene Thermal Maximum and

776   Eocene-Oligocene transition, Climate of the Past 12, 819–835, 10.5194/cp-12-819-2016,

777   2016a.

778   22. Evans, D., Brierley, C., Raymo, M.E., Erez, J., and Müller, W.: Planktic foraminifera shell

779   chemistry response to seawater chemistry: Pliocene–Pleistocene seawater Mg/Ca,

780   temperature and sea level change, Earth and Planetary Science Letters 438, 139-148,

781   2016b, 10.1016/j.epsl.2016.01.013.

782   23. Fabbrini, A., Zaminga, I., Ezard, T. and Wade, B.S.: Systematic taxonomy of middle

783   Miocene *Sphaeroidinellopsis* (planktonic foraminifera), Journal of Systematic

784   Palaeontology, 19, 953-968, 10.1080/14772019.2021.1991500, 2021.

785   24. Fayolle, F. and Wade, B.S.: Data report: Miocene planktonic foraminifers

786   *Dentoglobigerina* and *Globoquadrina* from IODP Sites U1489 and U1490, Expedition

787   363. In: Rosenthal, Y., Holbourn, A.E., Kulhanek, D.K., and the Expedition 363 Scientists,

788   Western Pacific Warm Pool. Proceedings of the International Ocean Discovery Program,

789   363:   College   Station,   TX   (International   Ocean   Discovery   Program),

790   10.14379/iodp.proc.363.203.2020, 2020.

791   25. Friedrich, O., Schiebel, R., Wilson, P.A., Weldeab, S., Beer, C.J., Cooper, M.J., and Fiebig,

792   J.: Influence of test size, water depth, and ecology on Mg/Ca, Sr/Ca, δ18O and δ13C in

793   nine modern species of planktic foraminifers, Earth and Planetary Science Letters 319,

794   133-145, 10.1016/j.epsl.2011.12.002, 2012.

795 26. Fritz-Endres, T., and Fehrenbacher, J.: Preferential loss of high trace element bearing inner

796   calcite in foraminifera during physical and chemical cleaning, Geochemistry, Geophysics,

797   Geosystems, 22, e2020GC009419, 10.1029/2020GC009419, 2021.

798 27. Gaskell, D.E., and Hull, P.: Technical note: A new online tool for δ18O–temperature

799   conversions, Climate of the past 19, 1265-1274, 10.5194/cp-19-1265-2023, 2023.

800 28. Gaskell, D.E., Huber, M., O'Brien, C.L., Inglis, G.N., Acosta, R.P., Poulsen, C.J., and Hull,

801   P.M.: The latitudinal temperature gradient and its climate dependence as inferred from

802   foraminiferal 18O over the past 95 million years, Proceedings of the National Academy of

803   Science USA 119, e2111332119, 10.1073/pnas.2111332119, 2022.

804 29. Gray, W.R., and Evans, D.: Nonthermal influences on Mg/Ca in planktonic foraminifera:

805   A review of culture studies and application to the last glacial maximum, Paleoceanography

806   and Paleoclimatology 34, 306–315, 10.1029/2018PA003517, 2019.

807 30. Gray, W. R., Weldeab, S., Lea, D. W., Rosenthal, Y., Gruber, N., Donner, B., and Fischer,

808   G.: The effects of temperature, salinity, and the carbonate system on Mg/Ca in

809   *Globigerinoides ruber* (white): A global sediment trap calibration, Earth and Planetary

810   Science Letters 482, 607–620, 10.1016/j.epsl.2017.11.026, 2018.

811 31. Holland, K., Branson, O., Haynes, L.L., Honisch, B., Allen, K.A., Russell, A.D.,

812   Fehrenbacher, J.S., Spero, H.J., and Eggins S.M.: Constraining multiple controls on

813   planktic foraminifera Mg/Ca, Geochimica et Cosmochimica Acta 273, 116–136,

814   10.1016/j.gca.2020.01.015, 2020.

815   32. Hönisch, B., Allen, K.A., Lea, D.W., Spero, H.J., Eggins, S.M., Arbuszewski, J., deMeno-

816   cal, P., Rosenthal, Y., Russell, A.D., and Elderfield, H.: The influence of salinity on Mg/Ca

817   in planktic foraminifers – evidence from cultures, core-top sediments and complementary

818   δ18O, Geochim. Cosmochim. Acta 121, 196–213, 10.1016/j.gca.2013.07.028, 2013.

819   33. Huber, B.T., Petrizzo, M.R., Young, J., Falzoni, F., Gilardoni, S., Bown, P.R., and Wade,

820   B.S.: Pforams@mikrotax: A new online taxonomic database for planktonic foraminifera,

821   Micropalaeontology, 62: 429-438, 2016.

822   34. John, E.H., Staudigel, P.T., Buse, B., Lear, C.H., Pearson, P.N., and Slater, S.M.: Revealing

823   their true stripes: Mg/Ca banding in the Paleogene planktonic foraminifera genus

824   *Morozovella* and implications for paleothermometry, Paleoceanography and

825   Paleoclimatology, 38, e2023PA004652, 10.1029/2023PA004652, 2023.

826   35. Jonkers, L., de Nooijer, L.J., Reichart, G.-J., Zahn, R., and Brummer, G.-J.A.: Encrustation

827   and trace element composition of *Neogloboquadrina dutertrei* assessed from single

828   chamber analyses – implications for paleotemperature estimates, Biogeosciences, 9, 4851–

829   4860, 10.5194/bg-9-4851-2012, 2012.

830   36. Jonkers, L., Gopalakrishnan, A., Weßel, L., Chiessi, C. M., Groeneveld, J., Monien, P., et

831   al.: Morphotype and crust effects on the geochemistry of *Globorotalia inflata*,

832   Paleoceanography and Paleoclimatology 36, e2021PA004224, 10.1029/2021PA004224 ,

833   2021.

834   37. Kısakürek, B., Eisenhauer, A., Böhm, F., Garbe-Schönberg, D., and Erez, J.: Controls on

835   shell Mg/Ca and Sr/Ca in cultured planktonic foraminiferan, *Globigerinoides ruber*

836   (white), Earth and Planetary Science Letters 273, 260-269, 10.1016/j.epsl.2008.06.026,

837   2008.

838   38. LeGrande A.N., and Schmidt G.A.: Global gridded data set of the oxygen isotopic
839   composition in seawater, Geophys. Res. Lett. 33, L12604, 10.1029/2006GL026011, 2006.

840   39. Lea, D.W., Mashiotta, T.A., and Spero, H.J.: Controls on magnesium and strontium uptake
841   in planktonic foraminifera determined by live culturing, Geochimica et Cosmochimica
842   Acta 63, 2369-2379, 10.1016/S0016-7037(99)00197-0, 1999.

843   40. Lear, C.H., Rosenthal, Y., and Slowey, N.: Benthic foraminiferal Mg/Ca-
844   paleothermometry: A revised core-top calibration, Geochimica et Cosmochimica Acta 66,
845   3375-3387, 10.1016/S0016-7037(02)00941-9, 2002.

846   41. Leckie, R.M., Wade, B.S., Pearson, P.N., Fraass, A.J., King, D.J., Olsson, R.K., Premoli
847   Silva, I., Spezzaferri, S., and Berggren, W.A.: Taxonomy, biostratigraphy, and phylogeny
848   of Oligocene and early Miocene *Paragloborotalia* and *Parasubbotina*, in Wade, B.S.,
849   Olsson, R.K., Pearson, P.N., Huber, B.T. and Berggren, W.A., Atlas of Oligocene
850   Planktonic Foraminifera, Cushman Foundation of Foraminiferal Research, Special
851   Publication, No. 46, p. 125-178, 2018.

852   42. Locarnini, R. A., Mishonov, A.V., Antonov, J.I., Boyer, T.P., Garcia, H.E., Baranova,
853   O.K., Zweng, M.M., Paver, C.R., Reagan, J.R., Johnson, D.R., Hamilton, M., and Seidov,
854   D.: World Ocean Atlas 2013, Volume 1: Temperature. S. Levitus, Ed., A. Mishonov
855   Technical Ed.; NOAA Atlas NESDIS 73, 40 pp, 2013.

856   43. Lourens, L.J., Hilgen, F.J., Shackleton, N.J., Laskar, J., and Wilson, D.: The Neogene
857   Period. In: Gradstein, F.M., Ogg, J.G., Smith, A.G. (Eds.), Geological Time Scale 2004.
858   Cambridge University Press, pp. 409–440, 2004.

859   44. Malevich, S. B., Vetter, L., and Tierney, J. E.: Global Core Top Calibration of 18O in

860   Planktic Foraminifera to Sea Surface Temperature, Paleoceanography and

861   Paleoclimatology, 34, 1292–1315, 10.1029/2019PA003576, 2019.

862   45. Mathien-Blard, E., and Bassinot, F.: Salinity bias on the foraminifera Mg/Ca thermometry:

863   correction procedure and implications for past ocean hydrographic reconstructions,

864   Geochem. Geophys. Geosyst. 10, Q12011, 10.1029/2008GC002353, 2009.

865   46. McConnell, M.C., and Thunell, R.C.: Calibration of the planktonic foraminiferal Mg/Ca

866   paleothermometer: sediment trap results from the Guaymas Basin, Gulf of California.

867   Paleoceanography 20, PA2016, 10.1029/2004PA001077, 2005.

868   47. Miller, K.G., Kominz, M.A., Browning, J.V., Wright, J.D., Mountain, G.S., Katz, M.E.,

869   Sugarman, P.J., Cramer, B.S., Christie-Blick, N., and Pekar, S.F.: The Phanerozoic record

870   of global sea-level change, Science 310, 1293–1298, 10.1126/science.1116412, 2005.

871   48. Miller, K.G., Browning, J.V., Schmelz, W.J., Kopp, R.E., Mountain, G.S., Wright, J.D.:

872   Cenozoic sea-level and cryospheric evolution from deep-sea geochemical and continental

873   margin records, Science Advances 6, eaaz1346, 2020.

874   49. Morard, R., Darling, K.F., Weiner, A.K.M., Hassenrück, C., Vanni, C., Cordier, T., Henry,

875   N., Greco, M., Vollma, N.M., Milivojevic, T., Rahman, S.N., Siccha, M., Meilland, J.,

876   Jonkers, L., Quillévéré, F., Escarguel, G., Douady, C.J., de Garidel-Thoron, T., de Vargas,

877   C., and Kucera, M.: The global genetic diversity of planktonic foraminifera reveals the

878   structure of cryptic speciation in plankton, Biological Reviews, 10.1111/brv.13065, 2024.

879   50. Mucci, A.: Influence of temperature on the composition of magnesian calcite overgrowths

880   precipitated from seawater, Geochimica et Cosmochimica Acta 51, 1977-1984,

881   10.1016/0016-7037(87)90186-4, 1987.

882   51. Mucci, A., Morse, J.W.: The incorporation of Mg2+ and Sr2+ into calcite overgrowths:
883   influences of growth rate and solution composition, Geochimica et Cosmochimica Acta
884   47, 217-233, 10.1016/0016-7037(83)90135-7, 1983.

885   52. Nuernberg, D.: Magnesium in tests of *Neogloboquadrina pachyderma* sinistral from high
886   northern and southern latitudes, The Journal of Foraminiferal Research 25, 350-368,
887   10.2113/gsjfr.25.4.350, 1995.

888   53. Nürnberg, D., Bijma, J., and Hemleben, C.: Assessing the reliability of magnesium in
889   foraminiferal calcite as a proxy for water mass temperatures, Geochimica et Cosmochimica
890   Acta 60, 803-814, 10.1016/0016-7037(95)00446-7, 1996.

891   54. Opdyke, B.N., and Pearson, P.N.: Data report: geochemical analysis of multiple planktonic
892   foraminifer species at discrete time intervals, In: Haggerty, J.A., Premoli Silva, I., Rack,
893   F., and McNutt, M.K. (Eds.), Proceedings of the Ocean Drilling Program, Scientific
894   Results, 144, 993-995, 10.2973/odp.proc.sr.144.052.1995, 1995.

895   55. Pälike, H., Norris, R.D., Herrle, J.O., Wilson, P.A., Coxall, H.K., and Lear, C.H.,
896   Shackleton, N.J., Tripati, A.K., Wade, B.S.: The heartbeat of the Oligocene climate system,
897   Science 314, 1894–1898, 10.1126/science.1133822, 2006.

898   56. Pearson, P.N., Shackleton, N.J., and Hall, M.A.: Stable isotopic evidence for the sympatric
899   divergence of *Globigerinoides trilobus* and *Orbulina universa*, Journal of the Geological
900   Society, 154, 295–302, 10.1144/gsjgs.154.2.0295, 1997.

901   57. Pearson, P.N.: Oxygen isotopes in foraminifera: overview and historical review. In
902   Reconstructing Earth's Deep-Time Climate, Paleontological Society Papers Volume 18, L.
903   Ivany, B. Huber, Eds. (2012), pp. 1–38, 2012.

904 58. Pearson, P.N., Young, J., King, D.J., and Wade, B.S.: Biochronology and evolution of

905 *Pulleniatina* (planktonic foraminifera), Journal of Micropalaeontology, 42, 211–255,

906 10.5194/jm-42-211-2023, 2023.

907 59. Rae, J.W.B., Zhang, Y., Liu, X., Foster, G.L., Stoll, H.M., and Whiteford, D.M.:

908 Atmospheric CO2 over the past 66 million years from marine archives, Annual Review of

909 Earth and Planetary Sciences 49, 609–641, 10.1146/annurev-earth-082420-063026, 2021.

910 60. Regenberg, M., Regenberg, A., Garbe-Schönberg, D., and Lea, D.W.: Global dissolution

911 effects on planktonic foraminiferal Mg/Ca ratios controlled by the calcite-saturation state

912 of bottom waters, Paleoceanography, 29, 127–142, 10.1002/2013PA002492, 2014.

913 61. Rohling, E. J., Foster, G. L., Gernon, T. M., Grant, K. M., Heslop, D., Hibbert, F. D., et

914 al.: Comparison and synthesis of sea-level and deep-sea temperature variations over the

915 past 40 million years. Reviews of Geophysics, 60, e2022RG000775, 2022.

916 62. Rongstad, B.L., Marchitto, T.M., and Herguera, J.C.: Understanding the effects of

917 dissolution on the Mg/Ca paleothermometer in planktic foraminifera: Evidence from a

918 novel individual foraminifera method, Paleoceanography 32, 1386–1402,

919 10.1002/2017PA003179, 2017.

920 63. Rosenthal, Y., Bova, S., and Zhou, X.: A user guide for choosing planktic foraminiferal

921 Mg/Ca-temperature calibrations. Paleoceanography and Paleoclimatology 37,

922 e2022PA004413, 2022.

923 64. Russell, A.D., Honisch, B., Spero, H.J., Lea, D.W.: Effects of seawater carbonate ion

924 concentration and temperature on shell U, Mg, and Sr in cultured planktonic foraminifera,

925 Geochimica and Cosmochimica Acta 68, 4347–4361, 10.1016/j.gca.2004.03.013, 2004.

926   65. Sexton, P.E., Wilson, P.A., and Pearson, P.N.: Microstructural and geochemical

927   perspectives on planktic foraminiferal preservation: "Glassy" versus "Frosty", Geochem.

928   Geophys. Geosyst. 7, 10.1029/2006GC001291, 2006.

929   66. Schiebel, R., and Hemleben, C.: Planktic foraminifers in the modern ocean. Springer, 2017.

930   67. Spero, H.J., Bijma, J., Lea, D.W., Bemis, B.E.: Effect of seawater carbonate concentration

931   on foraminiferal carbon and oxygen isotopes, Nature 390, 497-500, 10.1038/37333, 1997.

932   68. Spezzaferri, S., Coxall, H.K., Olsson, R.K., and Hemleben, C.: Taxonomy, biostratigraphy

933   and phylogeny of Oligocene Globigerina, Globigerinella, and Quiltyella n. gen., in Wade,

934   B.S., Olsson, R.K., Pearson, P.N., Huber, B.T. and Berggren, W.A., Atlas of Oligocene

935   Planktonic Foraminifera, Cushman Foundation of Foraminiferal Research, Special

936   Publication, No. 46, p. 125-178, 2018.

937   69. Spratt, R.M., and Lisiecki, L.: A Late Pleistocene sea-level stack, Climate of the past 12,

938   1070-1092, 10.5194/cp-12-1079-2016, 2016.

939   70. Staudigel, P.T., John, E.H., Buse, B., Pearson, P.N., and Lear, C.H.: Apparent preservation

940   of primary foraminiferal Mg/Ca ratios and Mg-banding in recrystallized foraminifera,

941   Geology 50, 760–764, 10.1130/G49984.1, 2022.

942   71. Tierney, J.E., Malevich, S.B., Gray, W., Vetter, L., and Thirumalai, K.: Bayesian

943   calibration of the Mg/Ca paleothermometer in planktic foraminifera, Paleoceanography

944   and Paleoclimatology 34, 2005-2030, 10.1029/2019PA003744, 2019.

945   72. Urey, H.C.: The thermodynamic properties of isotopic substance, Journal of the Chemical

946   Society of London 1947, 562–581, 1947.

947   73. Urey, H.C. Oxygen isotopes in nature and in the laboratory, Science 108, 489–496, 1948.

948   74. Von Langen, P.J., Pak, D.K., Spero, H.J., and Lea, D.W.: Effects of temperature on Mg/Ca

949   in neogloboquadrinid shells determined by live culturing, Geochemistry, Geophysics,

950   Geosystems 6, 10.1029/2005GC000989, 2005.

951   75. Wade, B.S., Pearson, P.N., Berggren, W.A., and Pälike, H.: Review and revision of

952   Cenozoic tropical planktonic foraminiferal biostratigraphy and calibration to the

953   geomagnetic polarity and astronomical time scale, Earth-Science Reviews 104, 111-142,

954   10.1016/j.earscirev.2010.09.003, 2011.

955   76. Weiner, A.K.M., Weinkauf, M.F.G., Kurasawa, A., Darling, K.F., and Kucera, M.: Genetic

956   and morphometric evidence for parallel evolution of the *Globigerinella calida*

957   morphotype, Marine Micropaleontology 114, 19–35, 10.1016/j.marmicro.2014.10.003,

958   2015.

959   77. Westerhold, T., Marwan, N., Drury, A.J., Liebrand, D., Agnini, C., Anagnostou, E., Barnet,

960   J.S.K., Bohaty, S.M., Vleeschouwer, D.D., Florindo, F., Frederichs, T., Hodell, D.A.,

961   Holbourn, A. E., Kroon, D., Lauretano, V., Littler, K., Lourens, L.J., Lyle, M., Pälike, H.,

962   Röhl, U., Tian, J., Wilkens, R.H., Wilson, P.A., and Zachos, J.C.: Anastronomically dated

963   record of Earth's climate and its predictability over the last 66 million years, Science, 369,

964   1383–1387, 10.1126/science.aba6853, 2020.

965   78. Yu, J., Elderfield, H., Greaves, M., and Day, J.: Preferential dissolution of benthic

966   foraminiferal calcite during laboratory reductive cleaning, Geochemistry, Geophysics,

967   Geosystems 8, 10.1029/2006GC001571, 2007.

968   79. Zarkogiannis, S.D., Antonarakou, A., Tripati, A., Kontakiotis, G., Mortyn, P.G., Drinia,

969   H., and Greaves, M.: Influence of surface ocean density on planktonic foraminifera

970   calcification, Scientific Reports 9, 10.1038/s41598-018-36935-7, 2019.

971   80. Zeebe, R. E.: An explanation of the effect of sea water carbonate concentration on

972   foraminiferal oxygen isotopes, Geochimica, Cosmochimica, Acta 63, 2001–2007,

973   10.1016/S0016-7037(99)00091-5, 1999.

974   81. Zeebe, R.E., and Tyrrell, T.: History of carbonate ion concentration over the last 100

975   million years II: revised calculations and new data, Geochimica and Cosmochima Acta

976   257, 373–392, 10.1016/j.gca.2019.02.041, 2019.

977   82. Zhou, X., Rosenthal, Y., Haynes, L., Si W., Evans, D., Huang, K.-F., Honisch, B., and

978   Erez, J.: Planktic foraminiferal Na/Ca: A potential proxy for seawater calcium

979   concentration, Geochimica et Cosmochimica Acta 305, 306–322,

980   10.1016/j.gca.2021.04.012, 2021.